

1 **Geophysical imaging of the deep critical zone**
2 **architecture reveals the complex interplay between**
3 **hydrological and weathering processes in a volcanic**
4 **tropical catchment**

5 **Sylvain Pasquet¹, Jean Marçais², Jorden L. Hayes³, Peter B. Sak^{3,4}, Lin Ma⁵,**
6 **Jérôme Gaillardet¹**

7 ¹Université de Paris, Institut de physique du globe de Paris, CNRS, Paris, France

8 ²INRAE, UR RiverLy, Villeurbanne, France

9 ³Department of Earth Sciences, Dickinson College, Carlisle PA, USA

10 ⁴Earth and Environmental Systems Institute and Department of Geosciences, Pennsylvania State

11 University, University Park, PA, USA

12 ⁵University of Texas at El Paso, El Paso TX, USA

13 **Key Points:**

- 14 • A novel combination of geophysics, petrophysics and geostatistics is used to char-
15 acterize the architecture of the deep critical zone.
16 • Maps of regolith thickness and water table depth reveal a deeply weathered zone
17 that impacts the hydrologic functioning of the watershed.
18 • We highlight spatial organization patterns that call for going beyond "simple" hill-
19 slope representations of the CZ.

Abstract

The Critical Zone (CZ) evolves through weathering and erosion processes that shape landscapes and control the availability and quality of natural resources. Although many of these processes take place in the deep CZ ($\sim 10\text{-}100$ m), direct information about its architecture remain scarce. Near-surface geophysics offer cost-effective and minimally-intrusive alternatives to drilling that can provide information about the physical properties of the CZ. We propose a novel workflow combining geophysics, petrophysics and geostatistics to characterize the architecture of the CZ (i.e., weathering front and water table depths) at the catchment scale, on the volcanic tropical island of Basse-Terre (Guadeloupe, France). Our results highlight two spatial organizations patterns for the weathering front and the water table, one along the stream and one transverse to it. This illustrates the robustness and strong potential of the proposed workflow to study hydrological and weathering processes in the CZ.

1 Introduction

In the Anthropocene, human activities have become a major component of the Earth system, directly affecting the ecosystem services essential to the development of our societies. These services are mostly hosted within the Critical Zone (CZ), which extends from the lower atmosphere to the top of unweathered bedrock (NRC, 2001). The CZ evolves through physical, chemical, and biological weathering and erosion processes that shape landscapes and control the availability and quality of natural resources (Brantley et al., 2007). Many of these processes take place in the deeper parts of the CZ ($\sim 10\text{-}100$ m), involving complex interactions between rock, air, water and life (Rempe & Dietrich, 2018). The deep CZ is frequently described as a bottom-up sequence of increasingly weathered materials (Riebe et al., 2017). As bedrock is exhumed towards the surface, the release of stress (tectonic or topographic) leads to the opening of fractures (St. Clair et al., 2015) and the exposure of new primary minerals (e.g., feldspar and mica) (Ackerer et al., 2021). These fractures open and connect towards the surface, thus increasing porosity (Hayes et al., 2019; Callahan et al., 2020) and favoring infiltration of reactive meteoric waters and chemical weathering of the rock (Lebedeva & Brantley, 2020; Brantley & Lebedeva, 2021). Besides, channel incision produces lateral drainage of subsurface water, enhancing weathering through drying and oxidation of the top of the CZ (Rempe & Dietrich, 2014). Around the water table, higher concentrations of dissolved O_2 and CO_2 promote dissolution and oxidation reactions which consume primary minerals and release mineral nutrients (Gu, Rempe, et al., 2020; Gu, Heaney, et al., 2020). As weathering intensifies, the bedrock material loses much of its mechanical strength and turns into saprolite, a friable layer yet physically intact enough to retain the texture of the parent bedrock (Graham et al., 2010). Close to the surface, the precipitation of new, less soluble secondary phases (clays, oxides...) and the weakening of the rock structure through bioturbation processes eventually lead to the formation of soils (Wilford & Thomas, 2013). Saprolite and soil are commonly associated into a common unit called regolith (Anderson et al., 2011).

The formation of regolith, and its removal by erosion processes, shapes the structure of the deep CZ (i.e., regolith thickness, porosity and permeability) (Rempe & Dietrich, 2014). This structure in turns impacts groundwater storage, residence time and flow paths (Flinchum, Holbrook, Grana, et al., 2018; Kolbe et al., 2020). It is strongly linked to many socially-relevant issues, including flooding and run-off (Lana-Renault et al., 2007; Gu erin et al., 2019) which affect slope stability (Nevers et al., 2021). The depth of the water table is also tightly intertwined with the structure of the deep CZ (Wang et al., 2021). Its monitoring is essential to manage groundwater resource (Carri ere et al., 2018) and quality (Turkeltaub et al., 2020). Agricultural practices also strongly depend on this deep compartment, as it controls river base-flow (Hector et al., 2015), exchanges in the hyporheic zone (Floury et al., 2019), crop yield (Mahindawansa et al., 2018), root-

ing depth (Shi et al., 2021), diversity of microorganisms (Stumpp & Hose, 2013), and organic matter accumulation or leaching (Jeanneau et al., 2020). Water table levels also control the sustainability of wetlands (Bertrand et al., 2021), and at a larger scales directly impact climate through their connection to soil moisture and carbon storage across continents (Fan et al., 2013). Despite these motivations, our understanding of mechanisms controlling these processes remains limited by the difficulty of accessing the CZ at depth. Boreholes and piezometric wells are often used to image the architecture of the CZ and locate the water table, but data remain limited by costs, field access, spatial coverage and the destructive nature of such measurements (Hubbard & Linde, 2011; Mailhot et al., 2019; Holbrook et al., 2019).

Minimally-invasive surface-based geophysical methods can be used to fill spatial gaps between wells by producing higher lateral resolution and lower cost data (Hubbard & Linde, 2011; Parsekian et al., 2015). Over the past ten years, an increasing number of studies have used geophysical methods to characterize the architecture of the CZ (Olona et al., 2010; Befus et al., 2011; Pasquet, Bodet, Longuevergne, et al., 2015; St. Clair et al., 2015; Yaede et al., 2015; Orlando et al., 2016; Novitsky et al., 2018; Comas et al., 2019; Eppinger et al., 2021; Parsekian et al., 2021; Wang et al., 2021, 2022). The vast majority of these studies rely on seismic refraction tomography to estimate pressure-wave velocity (V_P) at the hillslope scale. This observable is sensitive to subsurface mechanical properties which vary according to changes of porosity, bulk density or water content (Pride, 2005). To disentangle the cumulative effects of these parameters, a growing number of studies have used petrophysical relationships so as to convert these geophysical measurements into quantitative estimates of subsurface properties (Holbrook et al., 2014; Flinchum, Holbrook, Rempe, et al., 2018; Gase et al., 2018; Callahan et al., 2020). In most cases, the authors assume dry subsurface conditions to estimate porosity, and do not take into account variations of water content in the vicinity of the water table. The water content information is often obtained by relying on additional geophysical or piezometric data (Linde et al., 2007; Buchanan & Triantafilis, 2009; Boucher et al., 2009; Hayes et al., 2019; Flinchum et al., 2019). Several recent studies have shown that information about the water content could be inferred by estimating shear wave velocity (V_S) along with V_P (Grelle & Guadagno, 2009; Pasquet, Bodet, Dhemaied, et al., 2015; Pasquet, Bodet, Longuevergne, et al., 2015; Flinchum et al., 2020). Indeed, V_S is by definition less sensitive to changes in water content (Biot, 1956a, 1956b), since shear waves do not propagate in fluids. Combining both velocities in a petrophysical inversion framework thus allows reducing the ambiguity between lithological and water content variations at depth. This approach, previously implemented to characterize shallow hydrothermal activity in Yellowstone (WY) (Pasquet et al., 2016), is applied here for the first time to study CZ processes.

We propose a novel workflow combining geophysics, petrophysics and geostatistics to characterize the catchment scale CZ architecture, namely its vertical weathering structure and its related water table position. We apply this framework on the volcanic tropical island of Basse-Terre (Guadeloupe, France). We process seismic data collected along 5 different profiles in a small (8 ha) forested watershed. For each of these profiles, we combine seismic refraction tomography (SRT) and multichannel analysis of surface waves (MASW) to simultaneously estimate V_P and V_S velocities from a single seismic data set. Using the petrophysical inversion framework presented by Pasquet et al. (2016), we then convert these velocities into spatial distributions of subsurface porosity and saturation. Both V_P and saturation values are used to characterize the vertical structure of the CZ and the water table position in the watershed. We then use ordinary kriging interpolation to produce subsurface maps of the weathering front and the water table across the entire catchment. The spatial distribution of the regolith thickness and the water table depth reveal a deeply weathered zone that consistently impacts the hydrologic functioning of this tropical watershed. Overall this study highlights the potential of this novel

125 workflow to investigate reactive and hydrological processes in the CZ with cost-effective,
 126 minimally-intrusive geophysical methods.

127 2 Site Description

128 The Quiock Creek watershed is a 8 ha headwater catchment located on the wind-
 129 ward side of Basse-Terre Island, the volcanic part of the Guadeloupe archipelago (France)
 130 in the Lesser Antilles (Figure 1). The catchment is monitored by the ObsErA observa-
 131 tory which is part of the OZCAR critical zone research infrastructure (Gaillardet et al.,
 132 2018) and is dedicated to the study of weathering and erosion processes in the CZ un-
 133 der tropical climates (Clergue et al., 2015; Gu erin et al., 2019; Dessert et al., 2015, 2020).
 134 Indeed, due the volcanic nature of the rock formations and the tropical climate of Guade-
 135 loupe, weathering rates (i.e., the rate of transformation of rock into saprolite and soil)
 136 are amongst the highest on the planet (Gaillardet et al., 2011). The Quiock catchment
 137 is fully representative of volcanic tropical landscapes which are known to be hotspots of
 138 nutrient production, biological productivity and soil CO₂ consumption by chemical weath-
 139 ering (Louvati & All egre, 1997; Dessert et al., 2001). The Quiock Creek is a small trib-

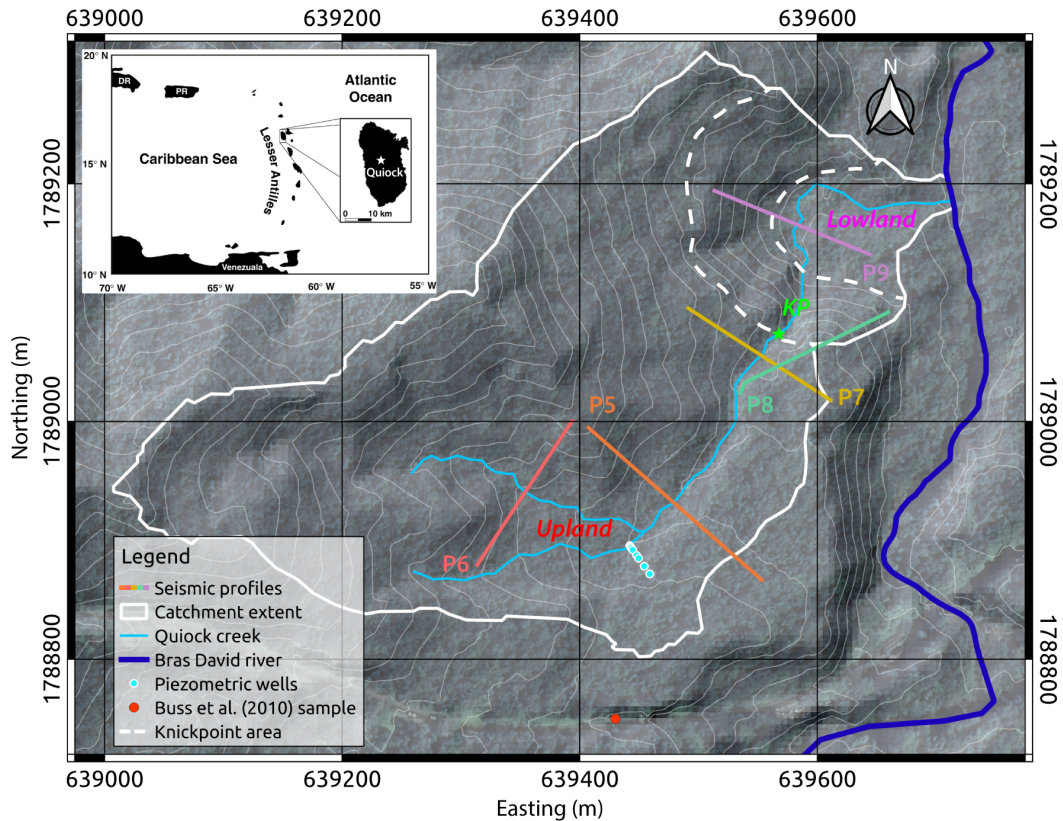


Figure 1. Topographic map of the studied area with 5-m elevation contours, showing the extent of the Quiock Creek watershed (white line) and the hydrological network (blue lines). Seismic profiles (colored lines), piezometric wells (light blue dots) and direct samples from Buss et al. (2010) (red dot) are also represented. The knickpoint area is delineated with dashed white line, and its location along the stream is shown with a green star. This map, and the following, are projected in the Universal Transverse Mercator geographic coordinate system, zone 20 N. The top left inset shows the location of Basse-Terre island in the Lesser Antilles.

140 utary of the Bras David river and is located in the primary tropical rainforest of Guade-
141 loupe National Park with mean annual temperature of 25°C. The elevation of the catch-
142 ment ranges from 200 m to 350 m and includes an active river knickpoint (i.e., sharp con-
143 vexity in an otherwise concave-up longitudinal river profile). The knickpoint is located
144 at ~250 m upstream of the confluence with the Bras David river and separates region-
145 ally extensive low relief surface upstream of the knickpoint, from more deeply incised streams
146 downstream (Sak et al., 2018). The hydrology of the site is strongly influenced by trop-
147 ical storms and hurricanes, with mean annual precipitation of 3500 mm/yr, evapotran-
148 spiration between 60 and 70%, and runoff of 1130 mm/yr (Dessert et al., 2020). Water
149 table levels are continuously monitored upstream of the knickpoint with pressure trans-
150 ducers installed in 7 piezometric wells arranged along a 30-m linear transect perpendic-
151 ular to the stream (Figure 1) and vary between 0.1 m and 4.1 m in the farthest well. The
152 catchment lies within Pleistocene andesitic pyroclastic deposits (Boudon et al., 1988) that
153 are weathered into a very thick regolith profile with ferralitic soils at the surface (Buss
154 et al., 2010). This weathering profile is highly depleted in mobile elements (Clergue et
155 al., 2015) and is mainly constituted of secondary minerals, with about 66% clay (hal-
156 loysite and kaolinite) and 28% iron and aluminum hydroxides (magnetite, goethite, maghemite
157 and gibbsite), minor amounts of primary minerals (mostly quartz and cristobalite) mak-
158 ing up the rest of the regolith composition. Bulk density measured in auger samples in
159 the upper 5 m is particularly low, on average $\sim 1 \text{ g.cm}^{-3}$ (Buss et al., 2010).

160 3 Material and Methods

161 3.1 Seismic Data Acquisition and Processing

162 Seismic data were first collected in May 2016 along a 188-m-long profile (P5) cross-
163 ing the Quiock Creek near the piezometric wells (Figure 1). Four supplemental 142-m-
164 long profiles (P6 to P9) were collected in May 2019, both up and downstream from the
165 original P5 transect. For each profile, P-wave first arrival times were picked manually,
166 then inverted for subsurface P-wave velocity (V_P) structure using the seismic refraction
167 tomography (SRT) code included in the Python geophysical inversion and modelling li-
168 brary pyGIMLI (Rücker et al., 2017). The program starts with an initial 2D model con-
169 sisting of a velocity field that increases linearly with depth, and then finds an appropri-
170 ately smooth update to the model that reduces the difference between predicted and ob-
171 served traveltimes (more details in the supporting information). These traveltimes are
172 compared for each source-receiver pair to check the quality of the inversion (Figure S1
173 in the supporting information). Velocity uncertainties (Figure S2) were estimated by run-
174 ning 144 inversions for each profile, using a different set of starting model and regular-
175 ization parameters for each inversion run (St. Clair et al., 2015; Pasquet et al., 2016).
176 The 144 inverted models are merged to build an average velocity model describing the
177 V_P distribution at depth along each profile (Figure 2b-2f).

178 The seismic data were also processed to perform multichannel analysis of surface-
179 waves (MASW) using the SWIP software package (Pasquet & Bodet, 2017). SWIP uses
180 spatial windowing and spectral stacking techniques (Neduczka, 2007; O’Neill et al., 2003)
181 to extract surface-wave dispersion data from the seismic records and retrieve a 2D model
182 of shear-wave velocity (V_S) from a succession of 1D inversions. We specifically apply the
183 novel multiwindow weighted stacking of surface-wave procedure (Pasquet et al., 2020)
184 to extract higher quality dispersion data and improve both the lateral resolution and depth
185 of investigation of the models (more details in the supporting information). Dispersion
186 curves are picked manually along each profile, and then inverted using the neighborhood
187 algorithm (NA) with the open software package Geopsy (Wathelet et al., 2004). For each
188 extracted dispersion curve, the NA inversion procedure generates 25000 models which
189 are used to build a 1D misfit-weighted final V_S model. The overall quality of these in-
190 versions is quantified by computing the residuals between observed and calculated dis-
191 persion curves along each profile (Figure S3). For each profile, all the consecutive 1D V_S

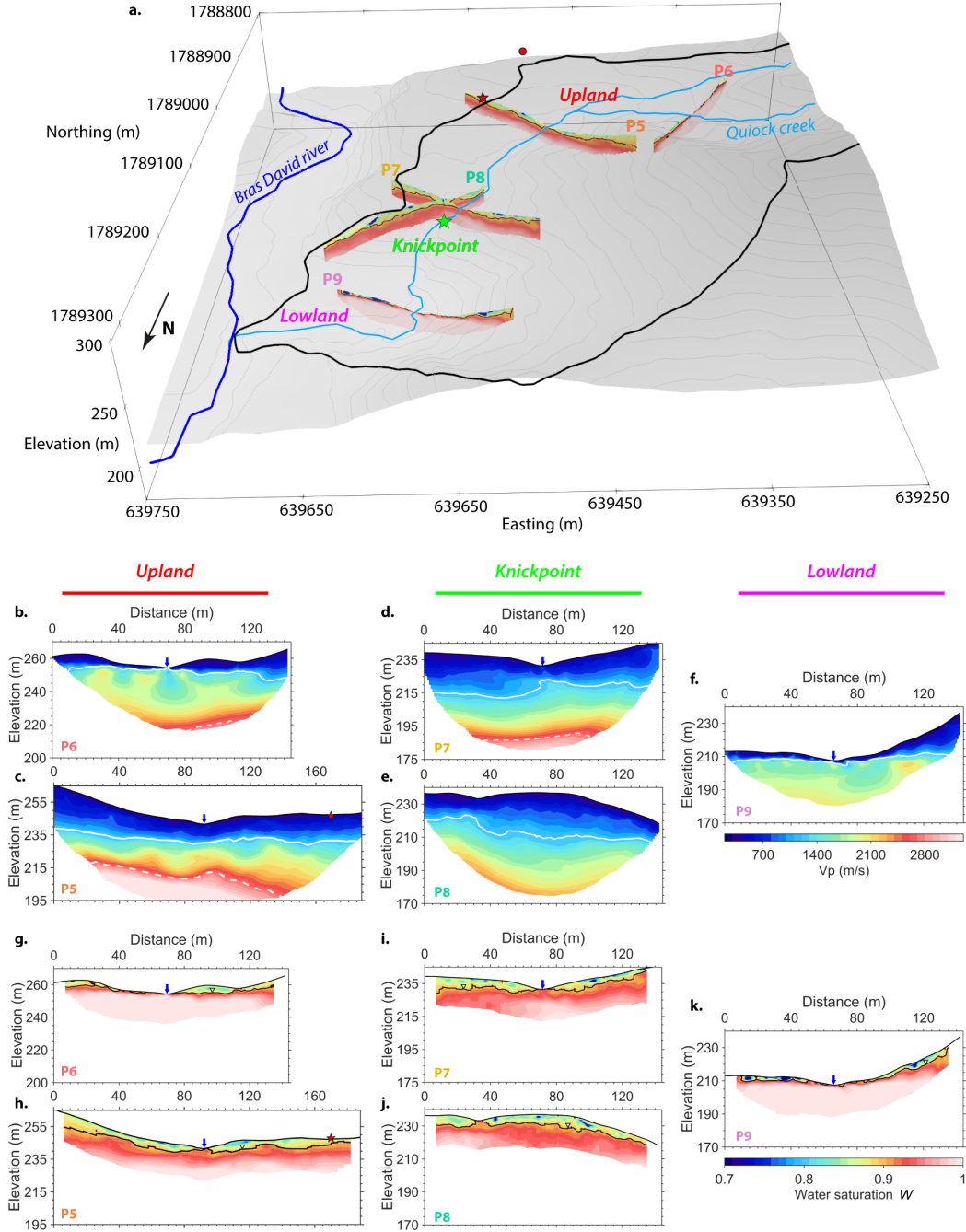


Figure 2. (a) 3D view of the inferred subsurface water saturation profiles in the Quiock catchment. The hydrological network (blue lines), the extent of the watershed (black line) and the location of the knickpoint (green star) are also represented. (b–f) P-wave velocity V_P and (g–k) water saturation profiles, with the blue arrows indicating the location of the stream. Horizontal distance = 0 m corresponds to the label position in (a). V_P contours corresponding to the bottom of sapolite (1200 m/s, white solid line) and the transition between weathered and fractured bedrock (2700 m/s, white dashed line) are shown in (b–f). Black contour lines in (g–k) correspond to the inferred water table ($W = 0.9$). The petrophysical model was calibrated by comparing soil sample analysis from Buss et al. (2010) (red dot in a) with the closest seismic data point at 170 m along P5 (red star in a, c and h).

192 models are finally assembled to create a 2D V_S section with the depth of investigation
 193 estimated from the uncertainties of each NA inversion (Figure S4).

194 3.2 Petrophysical Inversion

195 The inversion strategy relies on a petrophysical model based on Hertz-Mindlin con-
 196 tact theory (Mindlin, 1949) that describes the weathered regolith as a pack of spheri-
 197 cal beads. This is consistent with the textural description of highly weathered saprolite
 198 in tropical volcanic islands (White et al., 1998). With this model, we can express the bulk
 199 elastic properties of the regolith (i.e., bulk and shear moduli) as functions of the elas-
 200 tic properties of the minerals and fluids constituting the medium, and of their relative
 201 proportions (i.e., mineralogy, porosity and saturation). Here, we assume that all the beads
 202 in the model have an identical mineral composition that corresponds to the average com-
 203 position of the regolith (66% clay, 28% hydroxides and 6% quartz) observed in direct sam-
 204 ples collected at the site (Buss et al., 2010). A complete description of the model and
 205 the calibration of its parameters is given in the supporting information. The Hertz-Mindlin
 206 petrophysical model is then used in a grid search inversion scheme to look for the best
 207 set of porosity (Φ) and water saturation (W) values that minimizes the differences be-
 208 tween observed and modelled V_P and V_S (Figure S6), considering errors previously es-
 209 timated with SRT and MASW inversions. The grid search procedure was performed with
 210 porosity and saturation ranging between 0 and 1 in every cell of the 5 geophysical pro-
 211 files presenting valid values of both V_P and V_S . It allowed us to reconstruct 2D sections
 212 of porosity (Figure S7) and saturation (Figure 2g-2k), and evaluate their uncertainties
 213 (Figure S8).

214 3.3 Describing the Critical Zone Architecture

215 The depth of the interfaces between layers within the CZ can be estimated using
 216 the results of SRT. St. Clair et al. (2015) have pointed out that fresh bedrock is usually
 217 characterized by $V_P > 4000$ m/s, whereas fractured bedrock is expected to have $V_P >$
 218 2700 m/s in volcanic rocks (Adelinet et al., 2018). Several recent studies also described
 219 saprolite with $V_P < 1200$ m/s (Flinchum, Holbrook, Rempe, et al., 2018; Hayes et al.,
 220 2019). Soils express a large range of V_P which depends on their compaction and satu-
 221 ration levels, but generally show $V_P < 800$ m/s (Santamarina et al., 2005). However, when
 222 one of these interfaces lies in the vicinity of the water table, V_P is influenced by varia-
 223 tions of subsurface water content and can bias the estimation of the corresponding in-
 224 terface depth (Pasquet, Bodet, Dhemaied, et al., 2015). Here we propose to use the re-
 225 sults of the petrophysical inversion to map the depth of the water table and thus unbias
 226 the V_P -based estimation of the CZ interfaces. We define the depth of the water table when
 227 water saturation reaches a critical value (W_c) of 0.9, which corresponds to the top of the
 228 capillary fringe (de Marsily, 1986). We also consider an unbiased V_P -based estimation
 229 of a given interface depth as long as it is located below the water table (i.e., in fully sat-
 230 urated conditions).

231 While we could identify the saprolite-weathered bedrock interface ($V_P = 1200$ m/s)
 232 and the water table ($W = 0.9$) along all five seismic profiles collected in the Quiok catch-
 233 ment, the weathered to fractured bedrock interface ($V_P = 2700$ m/s) could only be de-
 234 tected in the three profiles collected upstream of the knickpoint (Figure 2). As the es-
 235 timated saprolite-weathered bedrock interface is systematically located under the wa-
 236 ter table (Figure 2), we consider that it is not biased by subsurface water content vari-
 237 ations. Soil thickness could not be precisely determined due to the large spacing between
 238 geophones (>2 m) used for both seismic campaigns, and is therefore not discussed fur-
 239 ther. In the following, soil and saprolite are undifferentiated and gathered within regolith.
 240 Similarly, the boundary between the bottom of regolith and the top of weathered bedrock
 241 is referred to as the weathering front.

3.4 Interpolating the Weathering Front and the Water Table

Since only the weathering front and the water table are clearly identified in all the seismic profiles, we focus the following section solely on reconstructing the 3D shape of these two interfaces across the catchment. We first extracted, from the digital elevation model (DEM) (Figure 3a), the spatial coordinates of these two interfaces at each point along the seismic profiles. We also added boundary conditions in the Bras David river to better constrain the interpolations, assuming: (i) a mean regolith thickness of 2 m that coincides with the most lowland values observed along P9 (Figure 2f), and (ii) a mean water level of 0.5 m, considering that the aquifer is directly connected to the river. We then used the GSTOOLS python library (Müller & Schüler, 2021) to interpolate the weathering front and the water table across the catchment (more details in the supporting information). We specifically applied ordinary kriging along a regular grid of 10x10 m cells covering the entire watershed in order to generate 3D surfaces of both the depth (i.e. vertical distance under the surface) and the elevation (i.e., vertical distance above sea level) of these interfaces. As shown by Snyder (2008), the water table position is better constrained by combining interpolations of both its depth and elevation. The interpolation of the water table elevation is more sensitive to the main trend associated with the regional hydrological gradient, whereas the interpolation of its depth helps reconstructing local perturbations associated with land surface irregularities. Following Snyder (2008), we used the average of these two interpolations to produce a map of the water table depth (Figure 3c) that incorporates both local and regional information. The same strategy was applied to interpolate the depth of the weathering front across the catchment (Figure 3b).

4 Results and Discussion

4.1 Characterization of the Critical Zone Architecture

In the upper 2-12 meters, V_P are mostly < 1200 m/s which is characteristic of clays constituting saprolite in highly weathered terrains such as those on Basse-Terre (Buss et al., 2010). As this 1200 m/s threshold is always located below the estimated water table (Figure 2), we consider that the estimation of the weathering front based on this threshold is not biased by variations of subsurface water content. The seismic data clearly underline a deepening of the weathering front in the knickpoint (Figure 2c-e), in comparison to upland and lowland areas (Figure 2b and 2f, respectively). The interpolated depth of the weathering front (Figure 3b) reveals a similar pattern, with a clear thickening of the regolith (> 15 m) in the vicinity of the knickpoint. In upland and lowland areas, the weathering front is closer to the surface at depths < 5 m. This particular organization is summarized in a synthetic cross-section (Figure 3f) where the depth of each interface identified in the seismic transects is represented along the topographic profile of the Quiock stream at their respective location (i.e., at the intersection or at the closest point in the stream).

The velocity threshold $V_P > 2700$ m/s, associated with the transition zone between weathered bedrock and fractured bedrock, is only reached upstream of the knickpoint (Figure 2b-d), at depths of about 40-50 m. Therefore it could not be interpolated across the whole catchment, and is only interpreted along the synthetic cross-section of the stream (Figure 3f). In the knickpoint (Figure 2e) and downstream of the knickpoint (Figure 2f), V_P is always < 2700 m/s over the whole investigated area, which goes as deep as 50 m in P8. Although we cannot image the base of the weathered bedrock in these areas, these results show that weathered bedrock extends at least down to 45 m in the lower end of the knickpoint, and down to 30 m in lowland areas. As no obvious deepening of the weathered-to-fractured bedrock transition zone is detected, we can hypothesize that this interface is located at a depth of about 40-50 m across the whole catchment, roughly following the landscape surface topography. Intact bedrock, usually described with velocities of 4000 m/s,

293 is never reached in the catchment, and is therefore located at depths > 50 m. Such a thick
 294 weathered zone is in good agreement with deep drilling observations made in similar trop-
 295 ical volcanic environment, where saprolite has been observed down to about 40 m (Buss
 296 et al., 2013).

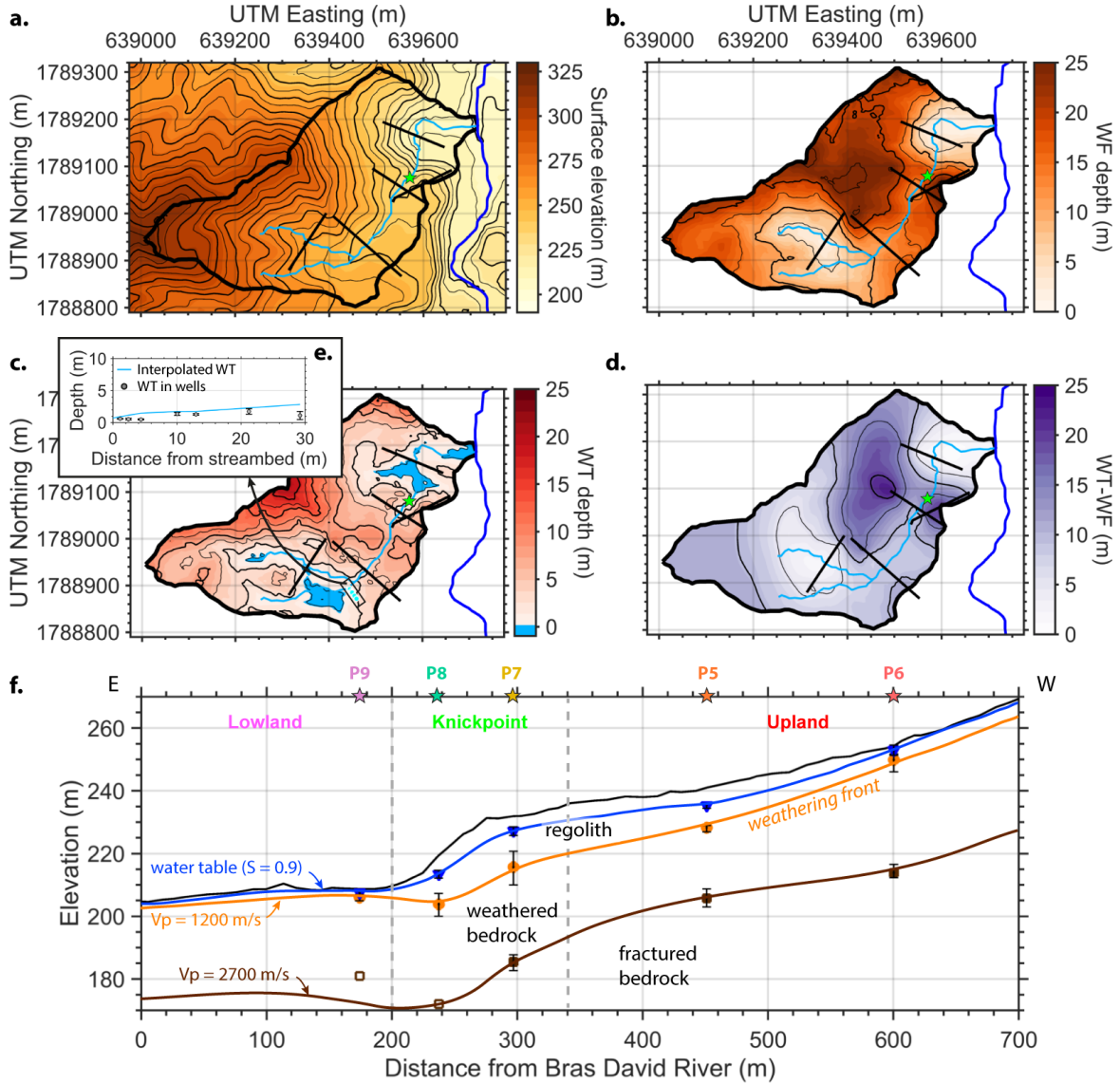


Figure 3. (a) DEM of the Quiock Creek watershed. (b) Interpolated depth of the weathering front (WF). (c) Interpolated depth of the water table (WT). (d) Difference between water table and weathering front elevations. These maps are overlaid with 5-m elevation/depth contours. The extent of the catchment and the seismic lines are shown in black, and the hydrological network in blue. (e) Comparison of average water table levels observed during the geophysical campaign in piezometric wells (light blue dots in c) with the corresponding interpolated water table depths. (f) Interpretive cross section of the stream topographic profile (black line) computed from the 5-m DEM. It highlights the location of the water table (in blue) and displays the structure of the CZ with specific V_P contours describing the weathering front (in orange), and the transition zone between weathered and fractured bedrock (in brown).

297 Inverted saturation cross sections provide estimates of water table levels that are
 298 consistent with field observations. Upstream of the knickpoint (Figure 2g-2i), the esti-
 299 mated water table outcrops at the intersections between the seismic profiles and the stream,
 300 in which water was flowing during the field campaign. The water table also outcrops in
 301 the small tributary crossed at the southern end of profile P8, whereas it goes deeper (~ 10 m)
 302 in the knickpoint (Figure 2j). Downstream of the knickpoint, the water table outcrops
 303 again widely (Figure 2k) in an area that was saturated during the May 2019 campaign.
 304 All these observations are consistent with the expected shape of the free water table in
 305 this small tropical catchment (Gu erin et al., 2019). Interpolated water table elevations
 306 (Figure S10) show a W-E trend that roughly follows the surface elevation gradient (Fig-
 307 ure 3a) oriented towards the Bras David river. This illuminates the overarching control
 308 that the Bras David river exerts on groundwater flow circulation in the Quiock catch-
 309 ment. Interpolated water table depths (Figure 3c) highlight three main seepage areas:
 310 (i) upstream of the knickpoint, before the junction of upper stream branches, (ii) just
 311 downstream of the knickpoint, and (iii) near the outlet. The depth to the top of the wa-
 312 ter table also increases beneath ridges, upstream and in the knickpoint (i.e., between pro-
 313 files P5 and P7). The estimated levels were compared to those observed in the piezomet-
 314 ric wells installed in the catchment (Gu erin et al., 2019). The observed water table lev-
 315 els were averaged over periods of one month centered on both field campaigns. These
 316 averaged piezometric levels show remarkably good agreement with water table levels in-
 317 terpolated with the average kriging approach (mean absolute error of 0.72 m) (Figure 3e).
 318 In comparison, water table levels interpolated solely with the elevations or the depths
 319 show significant deviation from the levels observed in piezometric wells (mean absolute
 320 errors of 0.74 m and 1.77 m, respectively) (Figure S11), confirming the robustness of the
 321 average kriging approach.

322 4.2 Implications for the Functioning of the Critical Zone

323 The joint characterization of the subsurface structure and water table depth in this
 324 tropical volcanic catchment sheds new light on reactive and hydrological processes gov-
 325 erning the functioning of the CZ. It appears that both the groundwater flow circulation
 326 and the regolith thickness are significantly impacted by the knickpoint. In upland area,
 327 far from the knickpoint, the water table appears to be classically controlled by the to-
 328 pography of the hillslope organization (Haitjema & Mitchell-Bruker, 2005) (Figure 3d-
 329 e). There, the water table is the deepest under the hill crest, at the water divide, and
 330 then rises up until meeting the land surface in the adjacent river. The weathering front
 331 follows the same organization, deeper under the hill crest than at the river ridges, although
 332 being always below the water table. On the contrary, just upstream of, and in the knick-
 333 point, the water table and the regolith thickness becomes completely disconnected from
 334 the surface, materializing a deepening of groundwater flow circulation concomitant with
 335 a thickening of the regolith (Figure 3f). Downstream of the knickpoint, in lowland ar-
 336 eas, the water table outcrops in vast saturated areas caused by the resurgence of ground-
 337 water flowpaths that originally come from upstream of the knickpoint (Figure 3c), as ma-
 338 terialized by the deepening of the water table. In lowland areas, the regolith becomes
 339 thinner, between 0 and 5 m. There, a shallow water table is likely to prevent deep in-
 340 filtration and rather favors shallow subsurface flowpaths, thus hindering regolith devel-
 341 opment (Weiler et al., 2006; Tromp-van Meerveld & McDonnell, 2006). Overall, the dif-
 342 ference between the water table and the weathering front (Figure 3d), appears to be spa-
 343 tially organized along the stream profile (i.e. following the knickpoint) rather than trans-
 344 verse to it (classical hillslope organization).

345 Two lateral organizations are thus structuring the catchment: one transverse from
 346 the hill crest towards the closest stream reach, and one longitudinal from the upland to
 347 the lowland area through the knickpoint. Understanding this particular organization,
 348 its impact on groundwater circulations, chemical weathering and erosion activity, requires
 349 to revisit evolution models coupling hydrology, weathering and erosion (Harman & Cosans,

2019; Braun et al., 2016; Brantley & Lebedeva, 2021). Indeed these hillslope models are
 intrinsically 2D, considering flowpaths from the hill crest to the river, and are thus un-
 able to simulate the complex 3D hydrological and reactive processes that lead to the CZ
 organization observed here.

4.3 Limitations and Challenges of the Workflow

A close examination of the petrophysical inversion residuals reveals that velocity
 distributions observed along P6 and P9 are not well reproduced at depth (Figure S6).
 This discrepancy is most likely due to the inability of the Hertz-Mindlin petrophysical
 model to correctly represent seismic velocities in high-velocity and less-weathered ma-
 terials. Yet, this does not impact our water table level estimates, as these are located
 above the poorly resolved areas. Another limitation of the modelling approach is the rel-
 ative lack of studies describing the elastic parameters of secondary minerals that con-
 stitute the regolith profile in the Quiocq catchment. For instance, we were only able to
 find a single publication reporting elastic parameters for iron oxides and hydroxides (Chicot
 et al., 2011). As an alternative, we could collect regolith samples at multiple locations
 along the seismic lines to estimate the bulk elastic parameters of the dry frame along with
 porosity and water content (Heap et al., 2021), so as to further constrain the petrophys-
 ical model. The proposed workflow could also be improved by collecting additional geo-
 physical data along the existing profiles. Incorporating electrical resistivity data into the
 petrophysical inversion framework would help constraining variations of clay content across
 the catchment, as this parameter is especially sensitive to the presence of water and clay,
 and can be modelled in rocks via Archie’s law (Archie, 1942) and its more advanced deriva-
 tives (Waxman & Smits, 1968; Glover, 2010; Jougnot et al., 2010).

The quality and robustness of the interpolation is sensitive to the number and den-
 sity of data points collected throughout the catchment. In this study we were only able
 to record five seismic profiles with data points unevenly distributed. As a result, the el-
 evations of the weathering front and the water table estimated in the outermost parts
 of the catchment are rather extrapolated than interpolated and thus only follow the main
 elevation and depth trends. We assume that the general trend of the elevation gradient
 used to extrapolate both weathering front and water table levels only remains valid within
 the catchment, and thus do not display the kriging results beyond the watershed (Fig-
 ure 3). Improving the density and coverage of data points across the catchment remains
 challenging in rugged and densely vegetated landscapes. Drilling additional piezomet-
 ric wells is costly and strictly regulated by Guadeloupe National Park policy. Deploy-
 ing extra seismic profiles across the catchment would help filling those gaps, yet requir-
 ing an improved methodology to optimize acquisition time and spatial coverage.

5 Conclusions

Using a novel combination of geophysics, petrophysics and geostatistics, we pro-
 vided an extended characterization of the CZ architecture. With a single geophysical sur-
 vey, we were able to map both the weathering front and the water table in a forested wa-
 tershed representative of tropical volcanic landscapes in the island of Basse-Terre (Guade-
 loupe, France). The proposed workflow uses seismic refraction tomography and multi-
 channel analysis of surface waves to retrieve 2D cross sections of P and S wave veloci-
 ties (V_P and V_S , respectively). While V_P were used to extract information about both
 the depths of the weathering front and the fractured bedrock, we combined V_P and V_S
 information in a petrophysical inversion framework to extract saturation values and high-
 light the position of the water table. We then used a kriging interpolation to infer spa-
 tial variation of both the weathering front and the water table across the catchment. The
 estimated water table levels are consistent with theoretical predictions and field obser-
 vations. Our results highlight a shallow water table (mostly < 5 m) and relatively thick

400 weathered zone (>15 m) in most parts of the catchment. Both the weathering front and
 401 the water table appear to be impacted by the knickpoint and deepen in its vicinity. The
 402 top of the fractured bedrock, when shallow enough to be detected, remains parallel to
 403 the topography at depths of about 45 m. This integrated view of the CZ architecture
 404 also highlights two main spatial organization patterns across the catchment: one trans-
 405 verse, along the hillslope, and one longitudinal, along the stream, strongly impacted by
 406 the knickpoint. These findings call for going beyond "simple" hillslope representations
 407 of the CZ when studying hydrological and weathering processes in such complex envi-
 408 ronments. These results also illustrate the robustness and strong potential of the pro-
 409 posed workflow for future critical zone studies.

410 Acknowledgements

411 We thank L. Bodet and UMR METIS at Sorbonne Université for lending part of
 412 the geophysical equipment, and E. Lajeunesse and the Obsera staff for running and main-
 413 taining the observatory's instrumentation and database. We are also grateful to A. Arènes,
 414 L. Derry, J. Druhan, M. Eichner, N. Fernandez, C. Le Traon and F. Levy for invaluable
 415 assistance during field work. This work was supported by the CRITEX ANR-11-EQPX-
 416 0011 project and NSF EAR Award No. 1251952.

417 Open Research

418 The seismic data used in this study are available on the H+ database which stores
 419 the geophysical data collected on the critical zone observatories of the OZCAR network.
 420 The data set can be accessed via https://doi.org/10.26169/hplus.obsera_seismic_data_2019.
 421

422 References

- 423 Ackerer, J., Ranchoux, C., Lucas, Y., Viville, D., Clément, A., Fritz, B., . . .
 424 Chabaux, F. (2021, November). Investigating the role of deep weathering
 425 in critical zone evolution by reactive transport modeling of the geochemi-
 426 cal composition of deep fracture water. *Geochimica et Cosmochimica Acta*,
 427 *312*, 257–278. Retrieved from [https://www.sciencedirect.com/science/](https://www.sciencedirect.com/science/article/pii/S001670372100435X)
 428 [article/pii/S001670372100435X](https://www.sciencedirect.com/science/article/pii/S001670372100435X) doi: 10.1016/j.gca.2021.07.017
- 429 Adelinet, M., Domínguez, C., Fortin, J., & Violette, S. (2018, January). Seismic-
 430 refraction field experiments on Galapagos Islands: A quantitative tool for
 431 hydrogeology. *Journal of Applied Geophysics*, *148*, 139–151. Retrieved from
 432 <http://www.sciencedirect.com/science/article/pii/S092698511730037X>
 433 doi: 10.1016/j.jappgeo.2017.10.009
- 434 Anderson, S. P., Anderson, R. S., Hinckley, E.-L. S., Kelly, P., & Blum, A. (2011,
 435 June). Exploring weathering and regolith transport controls on Critical Zone
 436 development with models and natural experiments. *Applied Geochemistry*, *26*,
 437 S3–S5. Retrieved from [http://www.sciencedirect.com/science/article/](http://www.sciencedirect.com/science/article/pii/S088329271100093X)
 438 [pii/S088329271100093X](http://www.sciencedirect.com/science/article/pii/S088329271100093X) doi: 10.1016/j.apgeochem.2011.03.014
- 439 Archie, G. (1942, December). The Electrical Resistivity Log as an Aid in Deter-
 440 mining Some Reservoir Characteristics. *Transactions of the AIME*, *146*(01),
 441 54–62. Retrieved from <https://doi.org/10.2118/942054-G> doi: 10.2118/
 442 942054-G
- 443 Befus, K. M., Sheehan, A. F., Leopold, M., Anderson, S. P., & Anderson, R. S.
 444 (2011, August). Seismic Constraints on Critical Zone Architecture, Boulder
 445 Creek Watershed, Front Range, Colorado. *Vadose Zone Journal*, *10*(3), 915–
 446 927. Retrieved from [https://dl.sciencesocieties.org/publications/vzj/](https://dl.sciencesocieties.org/publications/vzj/abstracts/10/3/915?search-result=1)
 447 [abstracts/10/3/915?search-result=1](https://dl.sciencesocieties.org/publications/vzj/abstracts/10/3/915?search-result=1) doi: 10.2136/vzj2010.0108

- 448 Bertrand, G., Ponçot, A., Pohl, B., Lhosmot, A., Steinmann, M., Johannet, A.,
 449 ... Toussaint, M.-L. (2021, February). Statistical hydrology for evalu-
 450 ating peatland water table sensitivity to simple environmental variables
 451 and climate changes application to the mid-latitude/altitude Frasne peat-
 452 land (Jura Mountains, France). *Science of The Total Environment*, 754,
 453 141931. Retrieved from [https://www.sciencedirect.com/science/article/
 454 pii/S0048969720354607](https://www.sciencedirect.com/science/article/pii/S0048969720354607) doi: 10.1016/j.scitotenv.2020.141931
- 455 Biot, M. A. (1956a, February). Theory of propagation of elastic waves in a
 456 fluid-saturated porous solid. II. Higher frequency range. *The Journal
 457 of the Acoustical Society of America*, 28(2), 179–191. Retrieved from
 458 <http://link.aip.org/link/?JAS/28/179/1> doi: 10.1121/1.1908241
- 459 Biot, M. A. (1956b, January). Theory of propagation of elastic waves in a fluid-
 460 saturated porous solid. I. Low-frequency range. *The Journal of the Acoustical
 461 Society of America*, 28(2), 168–178. Retrieved from [http://adsabs.harvard
 462 .edu/abs/1956ASAJ...28..168B](http://adsabs.harvard.edu/abs/1956ASAJ...28..168B) doi: 10.1121/1.1908239
- 463 Boucher, M., Favreau, G., Descloitres, M., Vouillamoz, J.-M., Massuel, S., Na-
 464 zoumou, Y., ... Legchenko, A. (2009, October). Contribution of geophysical
 465 surveys to groundwater modelling of a porous aquifer in semiarid Niger: An
 466 overview. *Comptes Rendus Geoscience*, 341(10), 800–809. Retrieved from
 467 <http://www.sciencedirect.com/science/article/pii/S1631071309001680>
 468 doi: 10.1016/j.crte.2009.07.008
- 469 Boudon, G., Dagain, J., Demet, M.-P., & Wetsercamp, D. (1988). *Notice explicative
 470 et carte géologique à 1/20 000 du Massif Volcanique de la Soufrière* (BRGM-
 471 CNRS- DRM-IPGP ed.).
- 472 Brantley, S. L., Goldhaber, M. B., & Ragnarsdottir, K. V. (2007, October). Cross-
 473 ing Disciplines and Scales to Understand the Critical Zone. *Elements*, 3(5),
 474 307–314. Retrieved from [https://pubs.geoscienceworld.org/elements/
 475 article-abstract/3/5/307/137740/Crossing-Disciplines-and-Scales-to
 476 -Understand-the](https://pubs.geoscienceworld.org/elements/article-abstract/3/5/307/137740/Crossing-Disciplines-and-Scales-to-Understand-the) doi: 10.2113/gselements.3.5.307
- 477 Brantley, S. L., & Lebedeva, M. I. (2021). Relating land surface, water ta-
 478 ble, and weathering fronts with a conceptual valve model for headwa-
 479 ter catchments. *Hydrological Processes*, 35(2), e14010. Retrieved from
 480 <http://onlinelibrary.wiley.com/doi/abs/10.1002/hyp.14010> (_eprint:
 481 <https://onlinelibrary.wiley.com/doi/pdf/10.1002/hyp.14010>) doi: [https://
 482 doi.org/10.1002/hyp.14010](https://doi.org/10.1002/hyp.14010)
- 483 Braun, J., Mercier, J., Guillocheau, F., & Robin, C. (2016). A simple model
 484 for regolith formation by chemical weathering. *Journal of Geophysical
 485 Research: Earth Surface*, 121(11), 2140–2171. Retrieved from [https://
 486 agupubs.onlinelibrary.wiley.com/doi/abs/10.1002/2016JF003914](https://agupubs.onlinelibrary.wiley.com/doi/abs/10.1002/2016JF003914) doi:
 487 10.1002/2016JF003914
- 488 Buchanan, S., & Triantafilis, J. (2009). Mapping Water Table Depth
 489 Using Geophysical and Environmental Variables. *Groundwater*,
 490 47(1), 80–96. Retrieved from [http://ngwa.onlinelibrary.wiley
 491 .com/doi/abs/10.1111/j.1745-6584.2008.00490.x](http://ngwa.onlinelibrary.wiley.com/doi/abs/10.1111/j.1745-6584.2008.00490.x) (_eprint:
 492 <https://onlinelibrary.wiley.com/doi/pdf/10.1111/j.1745-6584.2008.00490.x>)
 493 doi: 10.1111/j.1745-6584.2008.00490.x
- 494 Buss, H. L., Brantley, S. L., Scatena, F. N., Bazilievskaya, E. A., Blum, A.,
 495 Schulz, M., ... Cole, D. (2013). Probing the deep critical zone be-
 496 neath the Luquillo Experimental Forest, Puerto Rico. *Earth Surface
 497 Processes and Landforms*, 38(10), 1170–1186. Retrieved from [http://
 498 onlinelibrary.wiley.com/doi/abs/10.1002/esp.3409](http://onlinelibrary.wiley.com/doi/abs/10.1002/esp.3409) (_eprint:
 499 <https://onlinelibrary.wiley.com/doi/pdf/10.1002/esp.3409>) doi: 10.1002/
 500 esp.3409
- 501 Buss, H. L., White, A. F., Dessert, C., Gaillardet, J., Blum, A. E., & Sak, P. B.
 502 (2010). Depth profiles in a tropical, volcanic critical zone observatory: Basse-

- 503 Terre, Guadeloupe. In *Water-Rock Interaction - Proceedings of the 13th In-*
 504 *ternational Conference on Water-Rock Interaction, WRI-13* (pp. 245–248).
 505 Retrieved from [https://pennstate.pure.elsevier.com/en/publications/](https://pennstate.pure.elsevier.com/en/publications/depth-profiles-in-a-tropical-volcanic-critical-zone-observatory-b)
 506 [depth-profiles-in-a-tropical-volcanic-critical-zone-observatory-b](https://pennstate.pure.elsevier.com/en/publications/depth-profiles-in-a-tropical-volcanic-critical-zone-observatory-b)
- 507 Callahan, R. P., Riebe, C. S., Pasquet, S., Ferrier, K. L., Grana, D., Sklar,
 508 L. S., ... Holbrook, W. S. (2020). Subsurface Weathering Revealed
 509 in Hillslope-Integrated Porosity Distributions. *Geophysical Research*
 510 *Letters*, 47(15), e2020GL088322. Retrieved from <http://agupubs>
 511 [.onlinelibrary.wiley.com/doi/abs/10.1029/2020GL088322](http://agupubs.onlinelibrary.wiley.com/doi/abs/10.1029/2020GL088322) (_eprint:
 512 <https://onlinelibrary.wiley.com/doi/pdf/10.1029/2020GL088322>) doi:
 513 10.1029/2020GL088322
- 514 Carrière, S. D., Chalikakis, K., Ollivier, C., Heath, T., Mangin, M., Kempf, J., ...
 515 Lapègue, J. (2018, October). Sustainable groundwater resources exploration
 516 and management in a complex geological setting as part of a humanitarian
 517 project (Mahafaly Plateau, Madagascar). *Environmental Earth Sciences*,
 518 77(21), 734. Retrieved from <https://doi.org/10.1007/s12665-018-7909-1>
 519 doi: 10.1007/s12665-018-7909-1
- 520 Chicot, D., Mendoza, J., Zaoui, A., Louis, G., Lepingle, V., Roudet, F., & Lesage,
 521 J. (2011, October). Mechanical properties of magnetite (Fe₃O₄), hematite
 522 (α -Fe₂O₃) and goethite (α -FeO·OH) by instrumented indentation and molec-
 523 ular dynamics analysis. *Materials Chemistry and Physics*, 129(3), 862–
 524 870. Retrieved from [http://www.sciencedirect.com/science/article/](http://www.sciencedirect.com/science/article/pii/S0254058411004627)
 525 [pii/S0254058411004627](http://www.sciencedirect.com/science/article/pii/S0254058411004627) doi: 10.1016/j.matchemphys.2011.05.056
- 526 Clergue, C., Dellinger, M., Buss, H. L., Gaillardet, J., Benedetti, M. F., & Dessert,
 527 C. (2015, October). Influence of atmospheric deposits and secondary
 528 minerals on Li isotopes budget in a highly weathered catchment, Guade-
 529 loupe (Lesser Antilles). *Chemical Geology*, 414, 28–41. Retrieved from
 530 <http://www.sciencedirect.com/science/article/pii/S0009254115300152>
 531 doi: 10.1016/j.chemgeo.2015.08.015
- 532 Comas, X., Wright, W., Hynek, S. A., Fletcher, R. C., & Brantley, S. L. (2019).
 533 Understanding fracture distribution and its relation to knickpoint evo-
 534 lution in the Rio Icacos watershed (Luquillo Critical Zone Observa-
 535 tory, Puerto Rico) using landscape-scale hydrogeophysics. *Earth Sur-*
 536 *face Processes and Landforms*, 44(4), 877–885. Retrieved from <http://>
 537 onlinelibrary.wiley.com/doi/abs/10.1002/esp.4540 (_eprint:
 538 <https://onlinelibrary.wiley.com/doi/pdf/10.1002/esp.4540>) doi: 10.1002/
 539 esp.4540
- 540 de Marsily, G. (1986). *Quantitative Hydrogeology: Groundwater Hydrology for Engi-*
 541 *neers*. Academic Press.
- 542 Dessert, C., Clergue, C., Rousteau, A., Crispi, O., & Benedetti, M. F. (2020,
 543 January). Atmospheric contribution to cations cycling in highly weath-
 544 ered catchment, Guadeloupe (Lesser Antilles). *Chemical Geology*, 531,
 545 119354. Retrieved from [http://www.sciencedirect.com/science/article/](http://www.sciencedirect.com/science/article/pii/S0009254119304838)
 546 [pii/S0009254119304838](http://www.sciencedirect.com/science/article/pii/S0009254119304838) doi: 10.1016/j.chemgeo.2019.119354
- 547 Dessert, C., Dupré, B., François, L. M., Schott, J., Gaillardet, J., Chakrapani,
 548 G., & Bajpai, S. (2001, June). Erosion of Deccan Traps determined by
 549 river geochemistry: impact on the global climate and the 87Sr/86Sr ra-
 550 tio of seawater. *Earth and Planetary Science Letters*, 188(3), 459–474.
 551 Retrieved from [https://www.sciencedirect.com/science/article/](https://www.sciencedirect.com/science/article/pii/S0012821X0100317X)
 552 [pii/S0012821X0100317X](https://www.sciencedirect.com/science/article/pii/S0012821X0100317X) doi: 10.1016/S0012-821X(01)00317-X
- 553 Dessert, C., Lajeunesse, E., Lloret, E., Clergue, C., Crispi, O., Gorge, C., &
 554 Quidelleur, X. (2015, December). Controls on chemical weathering on
 555 a mountainous volcanic tropical island: Guadeloupe (French West In-
 556 dies). *Geochimica et Cosmochimica Acta*, 171, 216–237. Retrieved from
 557 <http://www.sciencedirect.com/science/article/pii/S0016703715005384>

- 558 doi: 10.1016/j.gca.2015.09.009
- 559 Eppinger, B. J., Hayes, J. L., Carr, B. J., Moon, S., Cosans, C. L., Hol-
560 brook, W. S., ... Plante, Z. T. (2021). Quantifying Depth-
561 Dependent Seismic Anisotropy in the Critical Zone Enhanced by
562 Weathering of a Piedmont Schist. *Journal of Geophysical Research:
563 Earth Surface*, 126(10), e2021JF006289. Retrieved from [http://
564 onlinelibrary.wiley.com/doi/abs/10.1029/2021JF006289](http://onlinelibrary.wiley.com/doi/abs/10.1029/2021JF006289) (_eprint:
565 <https://agupubs.onlinelibrary.wiley.com/doi/pdf/10.1029/2021JF006289>) doi:
566 10.1029/2021JF006289
- 567 Fan, Y., Li, H., & Miguez-Macho, G. (2013, February). Global Patterns of Ground-
568 water Table Depth. *Science*, 339(6122), 940–943. Retrieved from [https://
569 science.sciencemag.org.insu.bib.cnrs.fr/content/339/6122/940](https://science.sciencemag.org.insu.bib.cnrs.fr/content/339/6122/940) (Pub-
570 lisher: American Association for the Advancement of Science Section: Report)
571 doi: 10.1126/science.1229881
- 572 Flinchum, B. A., Banks, E., Hatch, M., Batelaan, O., Peeters, L. J. M., & Pas-
573 quet, S. (2020, September). Identifying recharge under subtle ephemeral
574 features in a flat-lying semi-arid region using a combined geophysical approach.
575 *Hydrology and Earth System Sciences*, 24(9), 4353–4368. Retrieved from
576 <https://hess.copernicus.org/articles/24/4353/2020/> (Publisher:
577 Copernicus GmbH) doi: <https://doi.org/10.5194/hess-24-4353-2020>
- 578 Flinchum, B. A., Holbrook, W. S., Grana, D., Parsekian, A. D., Carr, B. J., Hayes,
579 J. L., & Jiao, J. (2018, October). Estimating the water holding capacity of
580 the critical zone using near-surface geophysics. *Hydrological Processes*, 32(22),
581 3308–3326. Retrieved from [https://onlinelibrary.wiley.com/doi/abs/
582 10.1002/hyp.13260](https://onlinelibrary.wiley.com/doi/abs/10.1002/hyp.13260) doi: 10.1002/hyp.13260
- 583 Flinchum, B. A., Holbrook, W. S., Parsekian, A. D., & Carr, B. J. (2019, August).
584 Characterizing the Critical Zone Using Borehole and Surface Nuclear Mag-
585 netic Resonance. *Vadose Zone Journal*, 18(1). Retrieved from [https://
586 dl.sciencesocieties.org/publications/vzj/abstracts/18/1/180209](https://dl.sciencesocieties.org/publications/vzj/abstracts/18/1/180209)
587 doi: 10.2136/vzj2018.12.0209
- 588 Flinchum, B. A., Holbrook, W. S., Rempe, D., Moon, S., Riebe, C. S., Carr,
589 B. J., ... Peters, M. P. (2018). Critical Zone Structure Under a Gran-
590 ite Ridge Inferred From Drilling and Three-Dimensional Seismic Refraction
591 Data. *Journal of Geophysical Research: Earth Surface*, 123(6), 1317–1343.
592 Retrieved from [http://agupubs.onlinelibrary.wiley.com/doi/abs/
593 10.1029/2017JF004280](http://agupubs.onlinelibrary.wiley.com/doi/abs/10.1029/2017JF004280) doi: 10.1029/2017JF004280
- 594 Floury, P., Gaillardet, J., Tallec, G., Ansart, P., Bouchez, J., Louvat, P., & Gorge,
595 C. (2019). Chemical weathering and CO₂ consumption rate in a multilayered-
596 aquifer dominated watershed under intensive farming: The Orgeval Critical
597 Zone Observatory, France. *Hydrological Processes*, 33(2), 195–213. Retrieved
598 from <https://onlinelibrary.wiley.com/doi/abs/10.1002/hyp.13340> doi:
599 10.1002/hyp.13340
- 600 Gaillardet, J., Braud, I., Hankard, F., Anquetin, S., Bour, O., Dorfliger, N., ...
601 Zitouna, R. (2018, November). OZCAR: The French Network of Critical
602 Zone Observatories. *Vadose Zone Journal*, 17(1). Retrieved from [https://
603 dl.sciencesocieties.org/publications/vzj/abstracts/17/1/180067](https://dl.sciencesocieties.org/publications/vzj/abstracts/17/1/180067)
604 doi: 10.2136/vzj2018.04.0067
- 605 Gaillardet, J., Rad, S., Rivé, K., Louvat, P., Gorge, C., Allègre, C. J., & Lajeunesse,
606 E. (2011, December). Orography-driven chemical denudation in the Lesser
607 Antilles: Evidence for a new feed-back mechanism stabilizing atmospheric
608 CO₂. *American Journal of Science*, 311(10), 851–894. Retrieved from
609 <https://www.ajsonline.org/content/311/10/851> (Publisher: American
610 Journal of Science Section: Articles) doi: 10.2475/10.2011.02
- 611 Gase, A., Bradford, J., & Brand, B. (2018, January). Estimation of porosity and
612 water saturation in dual-porosity pyroclastic deposits from joint analysis of

- 613 compression, shear, and electromagnetic velocities. *Geophysics*, ID1–ID11. Re-
 614 trieved from <https://library.seg.org/doi/abs/10.1190/geo2017-0234.1>
 615 doi: 10.1190/geo2017-0234.1
- 616 Glover, P. W. J. (2010, November). A generalized Archie’s law for n phases. *GEO-*
 617 *PHYSICS*, 75(6), E247–E265. Retrieved from [https://library.seg.org/](https://library.seg.org/doi/full/10.1190/1.3509781)
 618 [doi/full/10.1190/1.3509781](https://library.seg.org/doi/full/10.1190/1.3509781) (Publisher: Society of Exploration Geophysi-
 619 cists) doi: 10.1190/1.3509781
- 620 Graham, R., Rossi, A., & Hubbert, R. (2010, February). Rock to regolith conver-
 621 sion: Producing hospitable substrates for terrestrial ecosystems. *GSA Today*,
 622 4–9. Retrieved from [http://www.geosociety.org/gsatoday/archive/20/2/](http://www.geosociety.org/gsatoday/archive/20/2/abstract/i1052-5173-20-2-4.htm)
 623 [abstract/i1052-5173-20-2-4.htm](http://www.geosociety.org/gsatoday/archive/20/2/abstract/i1052-5173-20-2-4.htm) doi: 10.1130/GSAT57A.1
- 624 Grelle, G., & Guadagno, F. M. (2009, July). Seismic refraction methodol-
 625 ogy for groundwater level determination: “Water seismic index”. *Jour-*
 626 *nal of Applied Geophysics*, 68(3), 301–320. Retrieved from [http://](http://www.sciencedirect.com/science/article/pii/S0926985109000202)
 627 www.sciencedirect.com/science/article/pii/S0926985109000202 doi:
 628 10.1016/j.jappgeo.2009.02.001
- 629 Gu, X., Heaney, P. J., Reis, F. D. A. A., & Brantley, S. L. (2020, October). Deep
 630 abiotic weathering of pyrite. *Science*, 370(6515). Retrieved from [http://](http://science.sciencemag.org/content/370/6515/eabb8092)
 631 science.sciencemag.org/content/370/6515/eabb8092 (Publisher: Ameri-
 632 can Association for the Advancement of Science Section: Research Article) doi:
 633 10.1126/science.abb8092
- 634 Gu, X., Rempe, D. M., Dietrich, W. E., West, A. J., Lin, T.-C., Jin, L., & Brantley,
 635 S. L. (2020, January). Chemical reactions, porosity, and microfracturing in
 636 shale during weathering: The effect of erosion rate. *Geochimica et Cosmochim-*
 637 *ica Acta*, 269, 63–100. Retrieved from [https://www.sciencedirect.com/](https://www.sciencedirect.com/science/article/pii/S0016703719306386)
 638 [science/article/pii/S0016703719306386](https://www.sciencedirect.com/science/article/pii/S0016703719306386) doi: 10.1016/j.gca.2019.09.044
- 639 Guérin, A., Devauchelle, O., Robert, V., Kitou, T., Dessert, C., Quiquerez,
 640 A., ... Lajeunesse, E. (2019). Stream-Discharge Surges Generated by
 641 Groundwater Flow. *Geophysical Research Letters*, 46(13), 7447–7455.
 642 Retrieved from [http://agupubs.onlinelibrary.wiley.com/doi/abs/](http://agupubs.onlinelibrary.wiley.com/doi/abs/10.1029/2019GL082291)
 643 [10.1029/2019GL082291](http://agupubs.onlinelibrary.wiley.com/doi/abs/10.1029/2019GL082291) doi: 10.1029/2019GL082291
- 644 Haitjema, H. M., & Mitchell-Bruker, S. (2005). Are Water Tables a Subdued Replica
 645 of the Topography? *Groundwater*, 43(6), 781–786. doi: 10.1111/j.1745-6584
 646 .2005.00090.x
- 647 Harman, C. J., & Cosans, C. L. (2019). A low-dimensional model of bedrock
 648 weathering and lateral flow coevolution in hillslopes: 2. Controls on weath-
 649 ering and permeability profiles, drainage hydraulics, and solute export
 650 pathways. *Hydrological Processes*, 33(8), 1168–1190. Retrieved from
 651 <http://onlinelibrary.wiley.com/doi/abs/10.1002/hyp.13385> doi:
 652 10.1002/hyp.13385
- 653 Hayes, J. L., Riebe, C. S., Holbrook, W. S., Flinchum, B. A., & Hartsough, P. C.
 654 (2019, September). Porosity production in weathered rock: Where volumetric
 655 strain dominates over chemical mass loss. *Science Advances*, 5(9), eaao0834.
 656 Retrieved from <https://advances.sciencemag.org/content/5/9/eaao0834>
 657 doi: 10.1126/sciadv.aao0834
- 658 Heap, M. J., Baumann, T. S., Rosas-Carbaljal, M., Komorowski, J.-C., Gilg, H. A.,
 659 Villeneuve, M., ... Reuschlé, T. (2021). Alteration-Induced Volcano Instability
 660 at La Soufrière de Guadeloupe (Eastern Caribbean). *Journal of Geophysi-*
 661 *cal Research: Solid Earth*, 126(8), e2021JB022514. Retrieved from [http://](http://onlinelibrary.wiley.com/doi/abs/10.1029/2021JB022514)
 662 onlinelibrary.wiley.com/doi/abs/10.1029/2021JB022514 (_eprint:
 663 <https://agupubs.onlinelibrary.wiley.com/doi/pdf/10.1029/2021JB022514>) doi:
 664 10.1029/2021JB022514
- 665 Hector, B., Séguis, L., Hinderer, J., Cohard, J.-M., Wubda, M., Descloitres, M., ...
 666 Boy, J.-P. (2015, October). Water storage changes as a marker for base flow
 667 generation processes in a tropical humid basement catchment (Benin): In-

- sights from hybrid gravimetry. *Water Resources Research*, 51(10), 8331–8361. Retrieved from <https://agupubs.onlinelibrary.wiley.com/doi/full/10.1002/2014WR015773> doi: 10.1002/2014WR015773
- Holbrook, W. S., Marcon, V., Bacon, A. R., Brantley, S. L., Carr, B. J., Flinchum, B. A., ... Riebe, C. S. (2019, March). Links between physical and chemical weathering inferred from a 65-m-deep borehole through Earth's critical zone. *Scientific Reports*, 9(1), 4495. Retrieved from <https://www.nature.com/articles/s41598-019-40819-9> doi: 10.1038/s41598-019-40819-9
- Holbrook, W. S., Riebe, C. S., Elwaseif, M., L. Hayes, J., Basler-Reeder, K., L. Harry, D., ... W. Hopmans, J. (2014, March). Geophysical constraints on deep weathering and water storage potential in the Southern Sierra Critical Zone Observatory. *Earth Surface Processes and Landforms*, 39(3), 366–380. Retrieved from <http://onlinelibrary.wiley.com/doi/10.1002/esp.3502/abstract> doi: 10.1002/esp.3502
- Hubbard, S. S., & Linde, N. (2011). Hydrogeophysics. In *Treatise on Water Science* (pp. 401–434). Elsevier. Retrieved from <http://www.sciencedirect.com/science/article/pii/B9780444531995000439>
- Jeanneau, L., Buysse, P., Denis, M., Gruau, G., Petitjean, P., Jaffrézic, A., ... Viaud, V. (2020, March). Water Table Dynamics Control Carbon Losses from the Destabilization of Soil Organic Matter in a Small, Lowland Agricultural Catchment. *Soil Systems*, 4(1), 2. Retrieved from <https://www.mdpi.com/2571-8789/4/1/2> (Number: 1 Publisher: Multidisciplinary Digital Publishing Institute) doi: 10.3390/soilsystems4010002
- Jougnot, D., Ghorbani, A., Revil, A., Leroy, P., & Cosenza, P. (2010, January). Spectral induced polarization of partially saturated clay-rocks: a mechanistic approach. *Geophysical Journal International*, 180(1), 210–224. Retrieved from <https://doi.org/10.1111/j.1365-246X.2009.04426.x> doi: 10.1111/j.1365-246X.2009.04426.x
- Kolbe, T., Marçais, J., Dreuzy, J.-R. d., Labasque, T., & Bishop, K. (2020). Lagged rejuvenation of groundwater indicates internal flow structures and hydrological connectivity. *Hydrological Processes*, 34(10), 2176–2189. Retrieved from <https://onlinelibrary.wiley.com/doi/abs/10.1002/hyp.13753> (_eprint: <https://onlinelibrary.wiley.com/doi/pdf/10.1002/hyp.13753>) doi: 10.1002/hyp.13753
- Lana-Renault, N., Latron, J., & Regüés, D. (2007, December). Streamflow response and water-table dynamics in a sub-Mediterranean research catchment (Central Pyrenees). *Journal of Hydrology*, 347(3), 497–507. Retrieved from <http://www.sciencedirect.com/science/article/pii/S0022169407005380> doi: 10.1016/j.jhydrol.2007.09.037
- Lebedeva, M. I., & Brantley, S. L. (2020). Relating the depth of the water table to the depth of weathering. *Earth Surface Processes and Landforms*, 45(9), 2167–2178. Retrieved from <https://onlinelibrary.wiley.com/doi/abs/10.1002/esp.4873> (_eprint: <https://onlinelibrary.wiley.com/doi/pdf/10.1002/esp.4873>) doi: 10.1002/esp.4873
- Linde, N., Revil, A., Bolève, A., Dagès, C., Castermant, J., Suski, B., & Voltz, M. (2007, February). Estimation of the water table throughout a catchment using self-potential and piezometric data in a Bayesian framework. *Journal of Hydrology*, 334(1), 88–98. Retrieved from <http://www.sciencedirect.com/science/article/pii/S0022169406005142> doi: 10.1016/j.jhydrol.2006.09.027
- Louvat, P., & Allègre, C. J. (1997, September). Present denudation rates on the island of Réunion determined by river geochemistry: Basalt weathering and mass budget between chemical and mechanical erosions. *Geochimica et Cosmochimica Acta*, 61(17), 3645–3669. Retrieved from <https://>

- 723 www.sciencedirect.com/science/article/pii/S0016703797001804 doi:
724 10.1016/S0016-7037(97)00180-4
- 725 Mahindawansa, A., Orlowski, N., Kraft, P., Rothfuss, Y., Racela, H., & Breuer,
726 L. (2018, August). Quantification of plant water uptake by water stable
727 isotopes in rice paddy systems. *Plant and Soil*, 429(1), 281–302.
728 Retrieved from <https://doi.org/10.1007/s11104-018-3693-7> doi:
729 10.1007/s11104-018-3693-7
- 730 Maillot, M., Flipo, N., Rivière, A., Desassis, N., Renard, D., Goblet, P., & Vin-
731 cent, M. (2019, November). Technical note: Water table mapping ac-
732 counting for river–aquifer connectivity and human pressure. *Hydrology*
733 *and Earth System Sciences*, 23(11), 4835–4849. Retrieved from [https://](https://hess.copernicus.org/articles/23/4835/2019/)
734 hess.copernicus.org/articles/23/4835/2019/ (Publisher: Copernicus
735 GmbH) doi: 10.5194/hess-23-4835-2019
- 736 Mindlin, R. D. (1949). Compliance of elastic bodies in contact. *Journal of Applied*
737 *Mechanics*, 16, 259–268.
- 738 Müller, S., & Schüler, L. (2021, July). *GeoStat-Framework/GSTools: v1.3.2 'Pure*
739 *Pink'*. Zenodo. Retrieved from <https://zenodo.org/record/5068979> (Lan-
740 guage: eng) doi: 10.5281/zenodo.5068979
- 741 Neduczka, B. (2007). Stacking of surface waves. *Geophysics*, 72(2), 51–58. Retrieved
742 from <http://link.aip.org/link/?GPY/72/V51/1> doi: 10.1190/1.2431635
- 743 Nevers, P., Bouchez, J., Gaillardet, J., Thomazo, C., Charpentier, D., Faure, L.,
744 & Bertrand, C. (2021, June). Landslides as geological hotspots of CO₂
745 emission: clues from the instrumented Séchilienne landslide, western Eu-
746 ropean Alps. *Earth Surface Dynamics*, 9(3), 487–504. Retrieved from
747 <https://esurf.copernicus.org/articles/9/487/2021/> (Publisher: Coper-
748 nicus GmbH) doi: 10.5194/esurf-9-487-2021
- 749 Novitsky, C. G., Holbrook, W. S., Carr, B. J., Pasquet, S., Okaya, D., & Flinchum,
750 B. A. (2018, January). Mapping inherited fractures in the Critical Zone using
751 seismic anisotropy from circular surveys. *Geophysical Research Letters*, 45(7),
752 3126–3135. Retrieved from [http://agupubs.onlinelibrary.wiley.com/doi/](http://agupubs.onlinelibrary.wiley.com/doi/abs/10.1002/2017GL075976)
753 [abs/10.1002/2017GL075976](http://agupubs.onlinelibrary.wiley.com/doi/abs/10.1002/2017GL075976) doi: 10.1002/2017GL075976
- 754 NRC. (2001). *Basic research opportunities in Earth Science*. Washington DC:
755 The National Academies Press. Retrieved from [https://www.nap.edu/](https://www.nap.edu/catalog/9981/basic-research-opportunities-in-earth-science)
756 [catalog/9981/basic-research-opportunities-in-earth-science](https://www.nap.edu/catalog/9981/basic-research-opportunities-in-earth-science) doi:
757 10.17226/9981
- 758 Olona, J., Pulgar, J., Fernández-Viejo, G., López-Fernández, C., & González-
759 Cortina, J. (2010, December). Weathering variations in a granitic
760 massif and related geotechnical properties through seismic and electri-
761 cal resistivity methods. *Near Surface Geophysics*, 8(6), 585–599. Re-
762 trieved from <http://www.earthdoc.org/detail.php?pubid=43265> doi:
763 10.3997/1873-0604.2010043
- 764 O'Neill, A., Dentith, M., & List, R. (2003, January). Full-waveform P-SV reflectiv-
765 ity inversion of surface waves for shallow engineering applications. *Exploration*
766 *Geophysics*, 34(3), 158–173. Retrieved from [http://www.publish.csiro.au/](http://www.publish.csiro.au/paper/EG03158)
767 [paper/EG03158](http://www.publish.csiro.au/paper/EG03158)
- 768 Orlando, J., Comas, X., Hynek, S. A., Buss, H. L., & Brantley, S. L. (2016). Archi-
769 tecture of the deep critical zone in the Río Icacos watershed (Luquillo Critical
770 Zone Observatory, Puerto Rico) inferred from drilling and ground penetrating
771 radar (GPR). *Earth Surface Processes and Landforms*, 41(13), 1826–1840. Re-
772 trieved from <http://onlinelibrary.wiley.com/doi/abs/10.1002/esp.3948>
773 ([_eprint: https://onlinelibrary.wiley.com/doi/pdf/10.1002/esp.3948](https://onlinelibrary.wiley.com/doi/pdf/10.1002/esp.3948)) doi:
774 10.1002/esp.3948
- 775 Parsekian, A. D., Grana, D., Neves, F. d. A., Pleasants, M. S., Seyfried, M.,
776 Moravec, B. G., ... Kelleners, T. (2021, February). Hydrogeophysical com-
777 parison of hillslope critical zone architecture for different geologic substrates.

- 778 *Geophysics*, 1–84. Retrieved from [https://library.seg.org/doi/abs/](https://library.seg.org/doi/abs/10.1190/geo2020-0438.1)
779 10.1190/geo2020-0438.1 (Publisher: Society of Exploration Geophysicists)
780 doi: 10.1190/geo2020-0438.1
- 781 Parsekian, A. D., Singha, K., Minsley, B. J., Holbrook, W. S., & Slater, L. (2015,
782 March). Multiscale geophysical imaging of the critical zone. *Reviews of Geo-*
783 *physics*, 53(1), 2014RG000465. Retrieved from [http://onlinelibrary.wiley](http://onlinelibrary.wiley.com/doi/10.1002/2014RG000465/abstract)
784 [.com/doi/10.1002/2014RG000465/abstract](http://onlinelibrary.wiley.com/doi/10.1002/2014RG000465/abstract) doi: 10.1002/2014RG000465
- 785 Pasquet, S., & Bodet, L. (2017, July). SWIP: An integrated workflow for surface-
786 wave dispersion inversion and profiling. *Geophysics*, 82(6), WB47–WB61.
787 Retrieved from <http://library.seg.org/doi/abs/10.1190/geo2016-0625.1>
788 doi: 10.1190/geo2016-0625.1
- 789 Pasquet, S., Bodet, L., Dhemaied, A., Mouhri, A., Vitale, Q., Rejiba, F., . . . Guérin,
790 R. (2015, February). Detecting different water table levels in a shallow aquifer
791 with combined P-, surface and SH-wave surveys: Insights from VP/VS or
792 Poisson’s ratios. *Journal of Applied Geophysics*, 113, 38–50. Retrieved from
793 <http://www.sciencedirect.com/science/article/pii/S0926985114003589>
794 doi: 10.1016/j.jappgeo.2014.12.005
- 795 Pasquet, S., Bodet, L., Longuevergne, L., Dhemaied, A., Camerlynck, C., Re-
796 jiba, F., & Guérin, R. (2015, August). 2D characterization of near-
797 surface VP/VS: surface-wave dispersion inversion versus refraction tomog-
798 raphy. *Near Surface Geophysics*, 13(4), 315–331. Retrieved from [http://](http://nsg.eage.org/publication/publicationdetails/?publication=81945)
799 nsg.eage.org/publication/publicationdetails/?publication=81945
800 doi: 10.3997/1873-0604.2015028
- 801 Pasquet, S., Holbrook, W. S., Carr, B. J., & Sims, K. W. W. (2016, December).
802 Geophysical imaging of shallow degassing in a Yellowstone hydrothermal sys-
803 tem. *Geophysical Research Letters*, 43(23), 2016GL071306. Retrieved from
804 <http://onlinelibrary.wiley.com/doi/10.1002/2016GL071306/abstract>
805 doi: 10.1002/2016GL071306
- 806 Pasquet, S., Wang, W., Chen, P., & Flinchum, B. A. (2020, December). Multi-
807 window weighted stacking of surface-wave dispersion. *Geophysics*, 86(2),
808 EN39–EN50. Retrieved from [https://library.seg.org/doi/full/10.1190/](https://library.seg.org/doi/full/10.1190/geo2020-0096.1)
809 [geo2020-0096.1](https://library.seg.org/doi/full/10.1190/geo2020-0096.1) (Publisher: Society of Exploration Geophysicists) doi:
810 10.1190/geo2020-0096.1
- 811 Pride, S. R. (2005, January). Relationships between seismic and hydrological prop-
812 erties. In *Hydrogeophysics* (pp. 253–290). Springer. Retrieved from [http://](http://link.springer.com/chapter/10.1007/1-4020-3102-5_9)
813 link.springer.com/chapter/10.1007/1-4020-3102-5_9
- 814 Rempe, D. M., & Dietrich, W. E. (2014, May). A bottom-up control on fresh-
815 bedrock topography under landscapes. *Proceedings of the National Academy*
816 *of Sciences*, 111(18), 6576–6581. Retrieved from [https://www.pnas.org/](https://www.pnas.org/content/111/18/6576)
817 [content/111/18/6576](https://www.pnas.org/content/111/18/6576) doi: 10.1073/pnas.1404763111
- 818 Rempe, D. M., & Dietrich, W. E. (2018, March). Direct observations of rock mois-
819 ture, a hidden component of the hydrologic cycle. *Proceedings of the National*
820 *Academy of Sciences*, 115(11), 2664–2669. Retrieved from [https://www.pnas](https://www.pnas.org/content/115/11/2664)
821 [.org/content/115/11/2664](https://www.pnas.org/content/115/11/2664) doi: 10.1073/pnas.1800141115
- 822 Riebe, C. S., Hahm, W. J., & Brantley, S. L. (2017, January). Controls on deep
823 critical zone architecture: a historical review and four testable hypotheses.
824 *Earth Surface Processes and Landforms*, 42(1), 128–156. Retrieved from
825 <http://onlinelibrary.wiley.com/doi/10.1002/esp.4052/abstract> doi:
826 10.1002/esp.4052
- 827 Rucker, C., Günther, T., & Wagner, F. M. (2017, December). pyGIMLi: An open-
828 source library for modelling and inversion in geophysics. *Computers & Geo-*
829 *sciences*, 109, 106–123. Retrieved from [http://www.sciencedirect.com/](http://www.sciencedirect.com/science/article/pii/S0098300417300584)
830 [science/article/pii/S0098300417300584](http://www.sciencedirect.com/science/article/pii/S0098300417300584) doi: 10.1016/j.cageo.2017.07
831 .011
- 832 Sak, P. B., Miller, S. R., Ma, L., & Gaillardet, J. (2018, November). Fluvial knick-

- 833 points and transient erosion on Basse-Terre, Guadeloupe, with implications for
834 estimates of chemical weathering. Indianapolis IN, USA: GSA. Retrieved from
835 <https://gsa.confex.com/gsa/2018AM/webprogram/Paper324209.html>
- 836 Santamarina, J. C., Rinaldi, V. A., Fratta, D., Klein, K. A., Wang, Y.-H., Cho,
837 G. C., & Cascante, G. (2005, January). A survey of elastic and elec-
838 tromagnetic properties of near-surface soils. In *Near-Surface Geophysics*
839 (pp. 71–88). Society of Exploration Geophysicists. Retrieved from
840 <http://library.seg.org/doi/abs/10.1190/1.9781560801719.ch4>
- 841 Shi, P., Huang, Y., Ji, W., Xiang, W., Evaristo, J., & Li, Z. (2021, April). Im-
842 pacts of deep-rooted fruit trees on recharge of deep soil water using sta-
843 ble and radioactive isotopes. *Agricultural and Forest Meteorology*, *300*,
844 108325. Retrieved from <http://www.sciencedirect.com/science/article/pii/S0168192321000083> doi: 10.1016/j.agrformet.2021.108325
- 845 Snyder, D. T. (2008). Estimated Depth to Ground Water and Configuration of the
846 Water Table in the Portland, Oregon Area.
847 doi: 10.3133/SIR20085059
- 848 St. Clair, J., Moon, S., Holbrook, W. S., Perron, J. T., Riebe, C. S., Martel, S. J.,
849 ... Richter, D. d. (2015, October). Geophysical imaging reveals topographic
850 stress control of bedrock weathering. *Science*, *350*(6260), 534–538. Re-
851 trieved from <http://www.sciencemag.org/content/350/6260/534> doi:
852 10.1126/science.aab2210
- 853 Stumpp, C., & Hose, G. C. (2013, November). The impact of water table draw-
854 down and drying on subterranean aquatic fauna in in-vitro experiments. *PLoS*
855 *ONE*, *8*(11), e78502. Retrieved from [http://dx.doi.org/10.1371/journal](http://dx.doi.org/10.1371/journal.pone.0078502)
856 [.pone.0078502](http://dx.doi.org/10.1371/journal.pone.0078502) doi: 10.1371/journal.pone.0078502
- 857 Tromp-van Meerveld, H. J., & McDonnell, J. J. (2006). Threshold Relations in Sub-
858 surface Stormflow: 1. A 147-Storm Analysis of the Panola Hillslope. *Water Re-*
859 *sources Research*, *42*(2), W02410. doi: 10.1029/2004WR003778
- 860 Turkeltaub, T., Ascott, M. J., Gooddy, D. C., Jia, X., Shao, M.-A., & Binley,
861 A. (2020). Prediction of regional-scale groundwater recharge and nitrate
862 storage in the vadose zone: A comparison between a global model and a
863 regional model. *Hydrological Processes*, *34*(15), 3347–3357. Retrieved
864 from <http://onlinelibrary.wiley.com/doi/abs/10.1002/hyp.13834>
865 (_eprint: <https://onlinelibrary.wiley.com/doi/pdf/10.1002/hyp.13834>) doi:
866 10.1002/hyp.13834
- 867 Wang, W., Chen, P., Dueker, K., Zhang, Y., Lee, E.-j., Mu, D., ... Jiao, J.
868 (2021). Coevolution of Weathering Front and Water Table. *Geophysi-*
869 *cal Research Letters*, *48*(20), e2021GL092916. Retrieved from [http://](http://onlinelibrary.wiley.com/doi/abs/10.1029/2021GL092916)
870 onlinelibrary.wiley.com/doi/abs/10.1029/2021GL092916 (_eprint:
871 <https://agupubs.onlinelibrary.wiley.com/doi/pdf/10.1029/2021GL092916>) doi:
872 10.1029/2021GL092916
- 873 Wang, W., Nyblade, A., Mount, G., Moon, S., Chen, P., Accardo, N.,
874 ... Brantley, S. L. (2022). 3D seismic anatomy of a water-
875 shed reveals climate-topography coupling that drives water flow-
876 paths and bedrock weathering. *Journal of Geophysical Research:*
877 *Earth Surface*, *n/a*(n/a), e2021JF006281. Retrieved from [http://](http://onlinelibrary.wiley.com/doi/abs/10.1029/2021JF006281)
878 onlinelibrary.wiley.com/doi/abs/10.1029/2021JF006281 (_eprint:
879 <https://agupubs.onlinelibrary.wiley.com/doi/pdf/10.1029/2021JF006281>) doi:
880 10.1029/2021JF006281
- 881 Wathelet, M., Jongmans, D., & Ohrnberger, M. (2004, November). Surface-wave
882 inversion using a direct search algorithm and its application to ambient
883 vibration measurements. *Near Surface Geophysics*, *2*(4), 211–221. Re-
884 trieved from <http://earthdoc.eage.org/detail.php?pubid=8129> doi:
885 10.3997/1873-0604.2004018

- 887 Waxman, M., & Smits, L. (1968, June). Electrical Conductivities in Oil-Bearing
888 Shaly Sands. *Society of Petroleum Engineers Journal*, 8(02), 107–122. Re-
889 trieved from <https://doi.org/10.2118/1863-A> doi: 10.2118/1863-A
- 890 Weiler, M., McDonnell, J. J., Tromp-van Meerveld, I., & Uchida, T. (2006). Sub-
891 surface Stormflow. In *Encyclopedia of Hydrological Sciences*. John Wiley
892 & Sons, Ltd. Retrieved from [http://onlinelibrary.wiley.com/doi/](http://onlinelibrary.wiley.com/doi/10.1002/0470848944.hsa119/abstract)
893 [10.1002/0470848944.hsa119/abstract](http://onlinelibrary.wiley.com/doi/10.1002/0470848944.hsa119/abstract)
- 894 White, A. F., Blum, A. E., Schulz, M. S., Vivit, D. V., Stonestrom, D. A., Larsen,
895 M., . . . Eberl, D. (1998). Chemical Weathering in a Tropical Watershed,
896 Luquillo Mountains, Puerto Rico: I. Long-Term Versus Short-Term Weath-
897 ering Fluxes. *Geochimica et Cosmochimica Acta*, 62(2), 209–226. doi:
898 [10.1016/S0016-7037\(97\)00335-9](https://doi.org/10.1016/S0016-7037(97)00335-9)
- 899 Wilford, J., & Thomas, M. (2013, September). Predicting regolith thick-
900 ness in the complex weathering setting of the central Mt Lofty Ranges,
901 South Australia. *Geoderma*, 206, 1–13. Retrieved 2019-12-18, from
902 <http://www.sciencedirect.com/science/article/pii/S0016706113001122>
903 doi: 10.1016/j.geoderma.2013.04.002
- 904 Yaede, J. R., McBride, J. H., Nelson, S. T., Park, C. B., Flores, J. A., Turnbull,
905 S. J., . . . Gardner, N. L. (2015, April). A geophysical strategy for measuring
906 the thickness of the critical zone developed over basalt lavas. *Geosphere*, 11(2),
907 514–532. Retrieved from [http://pubs.geoscienceworld.org/geosphere/](http://pubs.geoscienceworld.org/geosphere/article/11/2/514/132242/A-geophysical-strategy-for-measuring-the-thickness)
908 [article/11/2/514/132242/A-geophysical-strategy-for-measuring-the](http://pubs.geoscienceworld.org/geosphere/article/11/2/514/132242/A-geophysical-strategy-for-measuring-the-thickness)
909 [-thickness](http://pubs.geoscienceworld.org/geosphere/article/11/2/514/132242/A-geophysical-strategy-for-measuring-the-thickness) doi: 10.1130/GES01142.1

Figure 1.

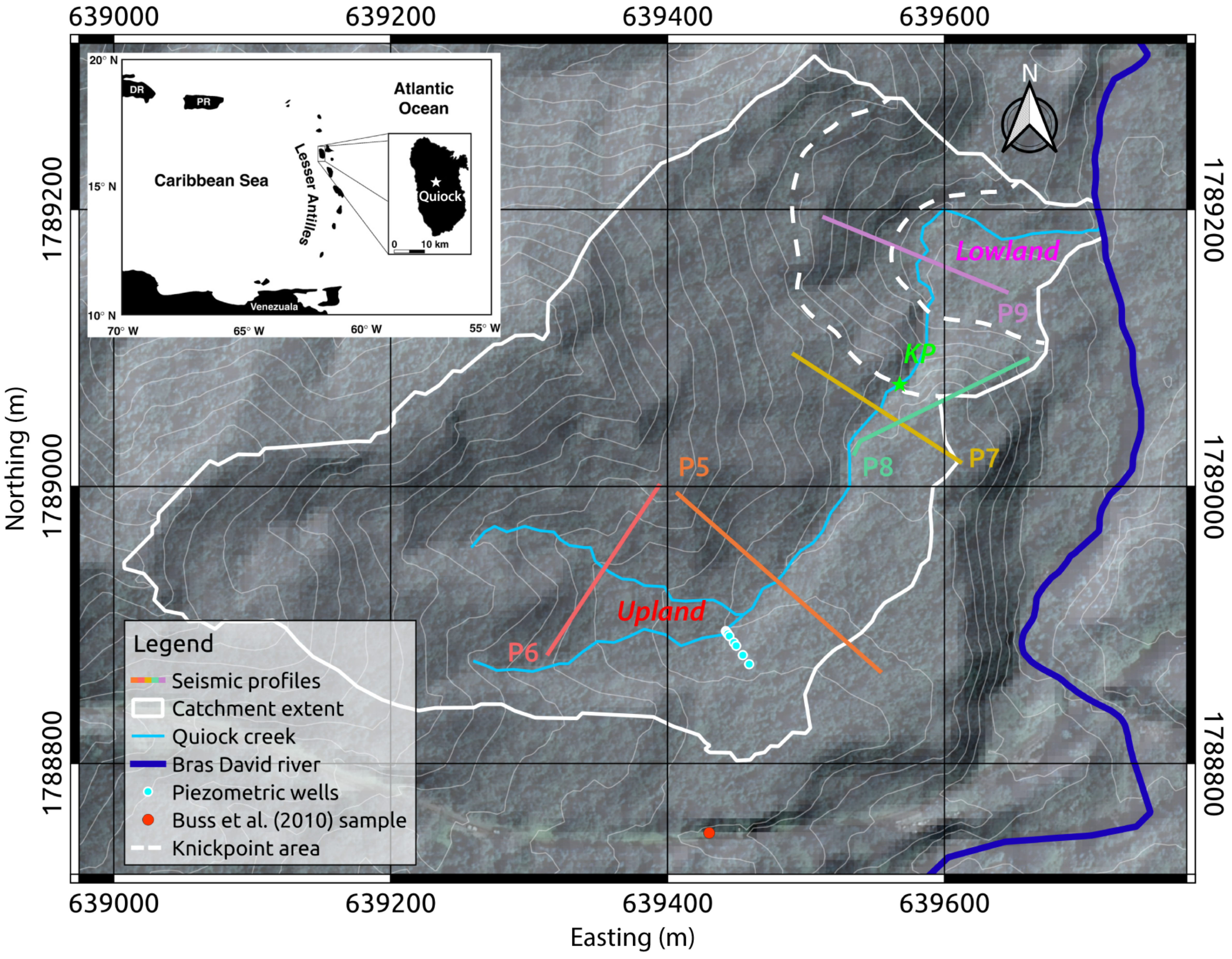
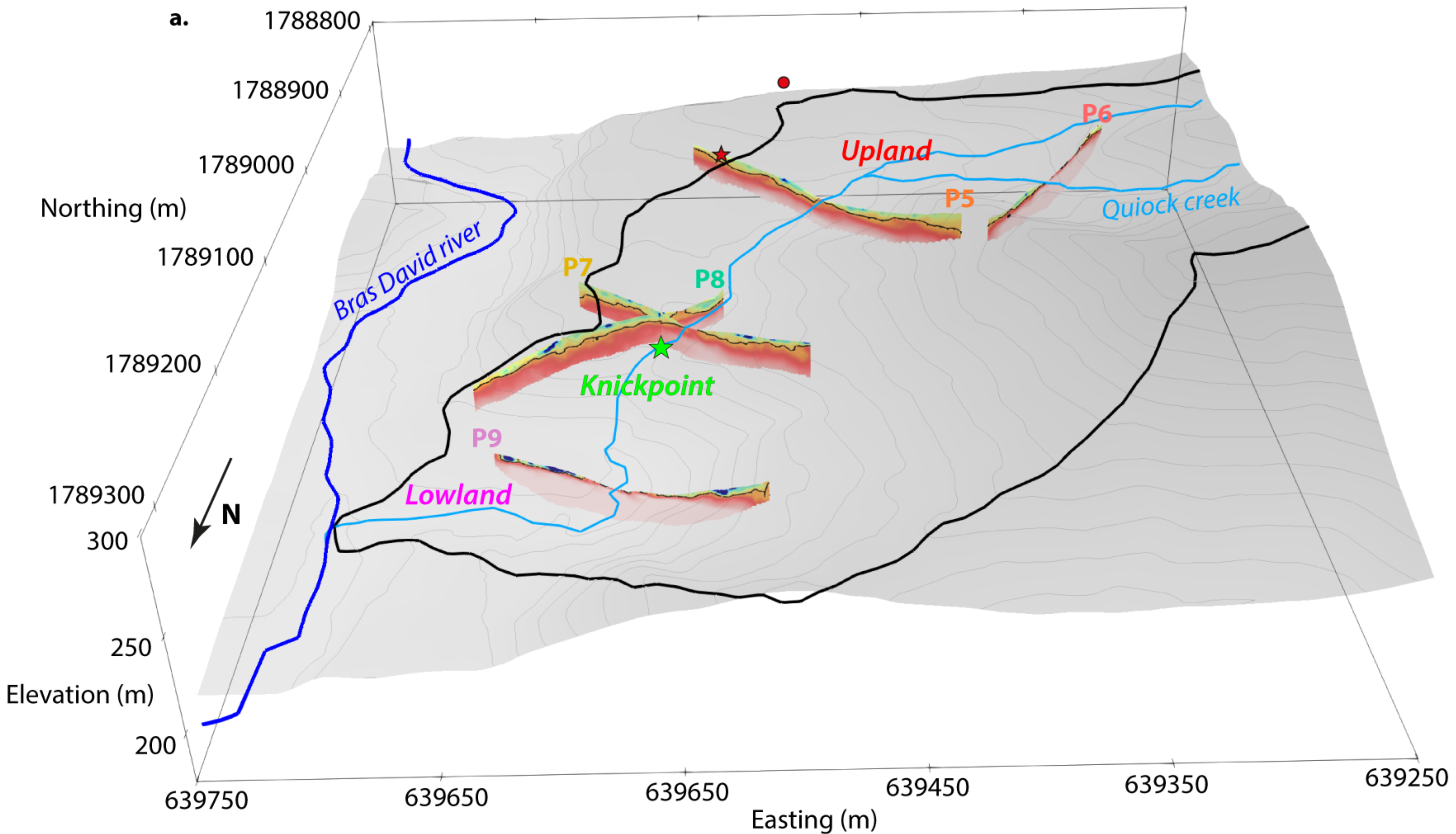


Figure 2.



Upland

Knickpoint

Lowland

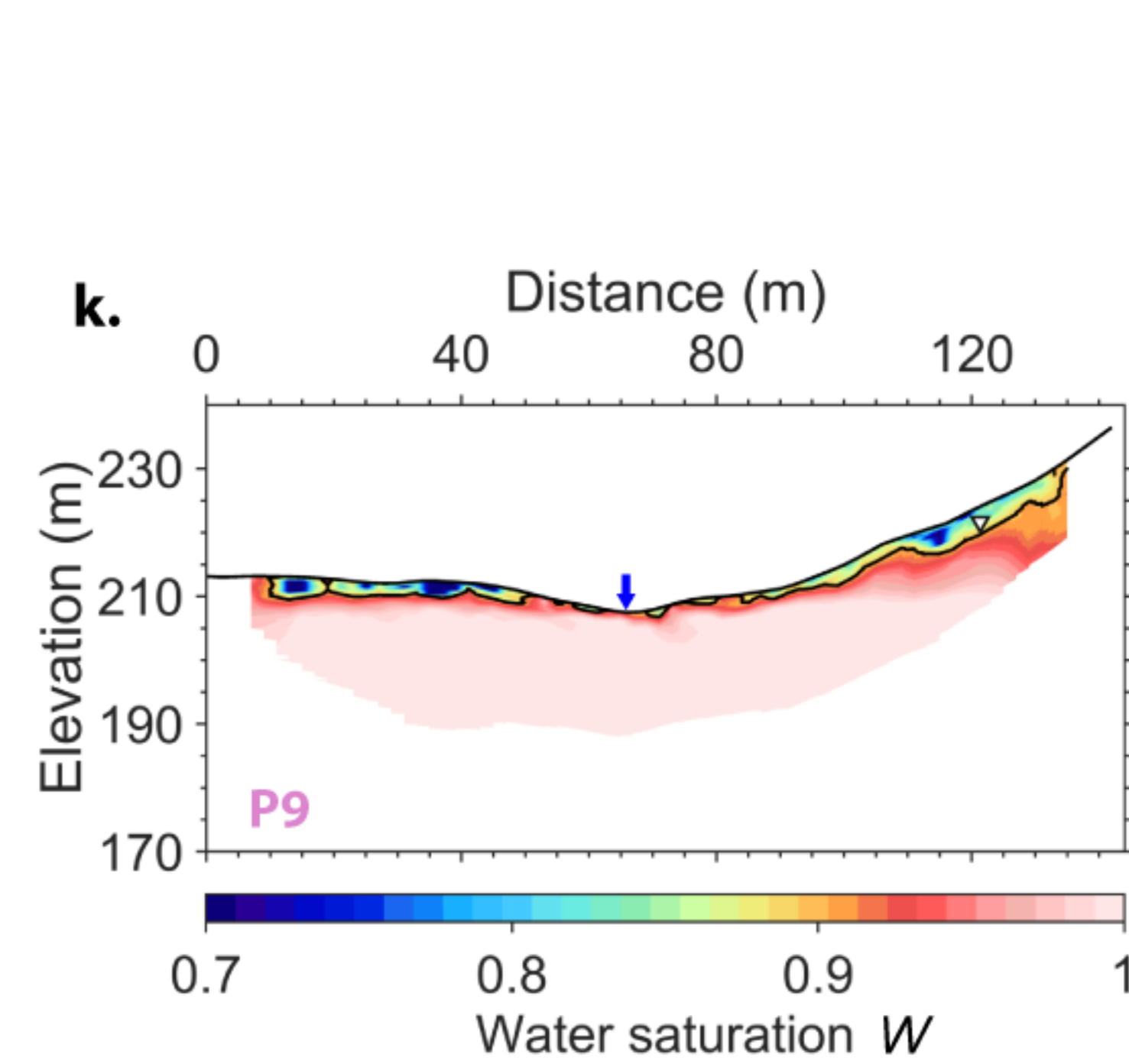
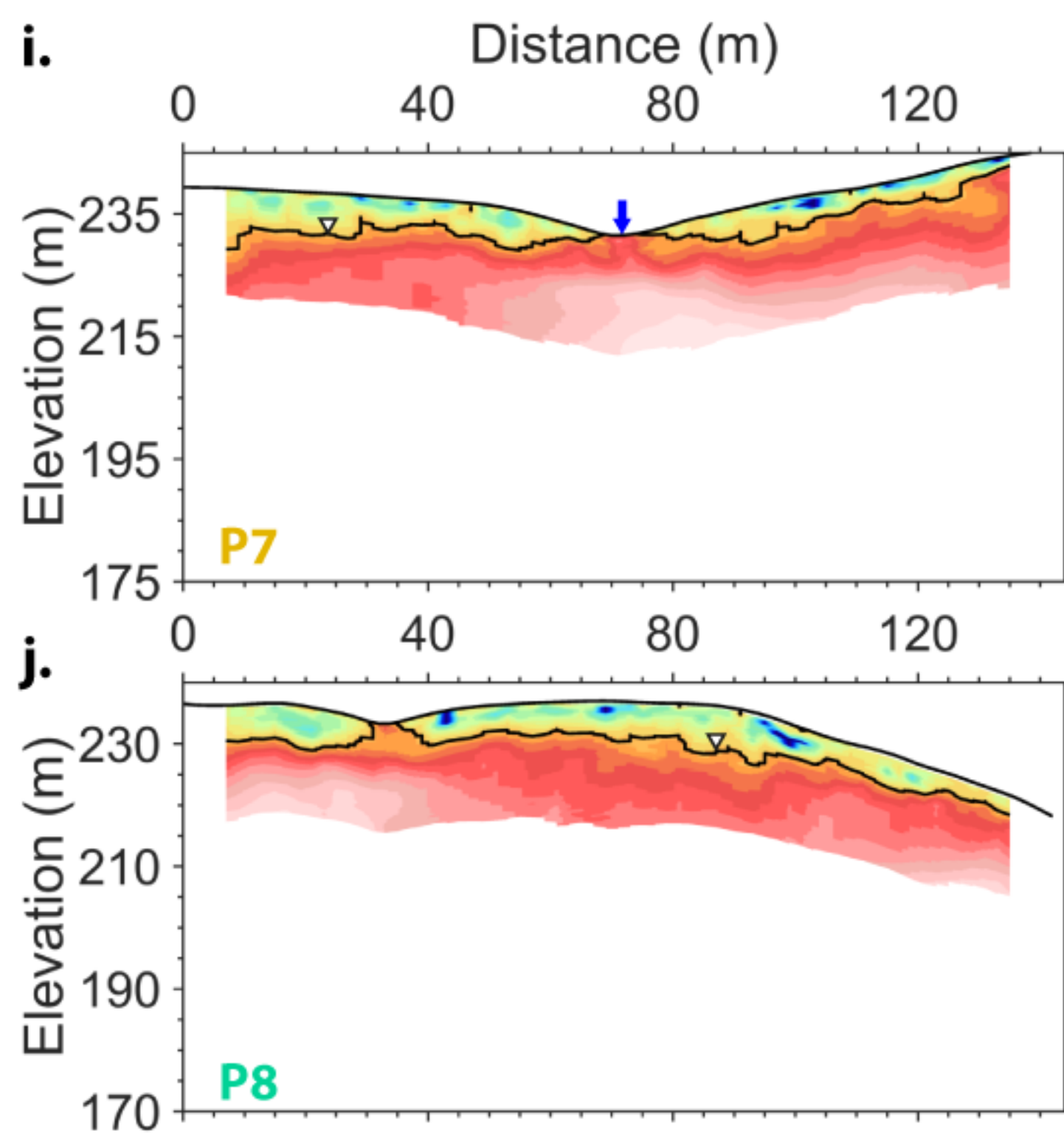
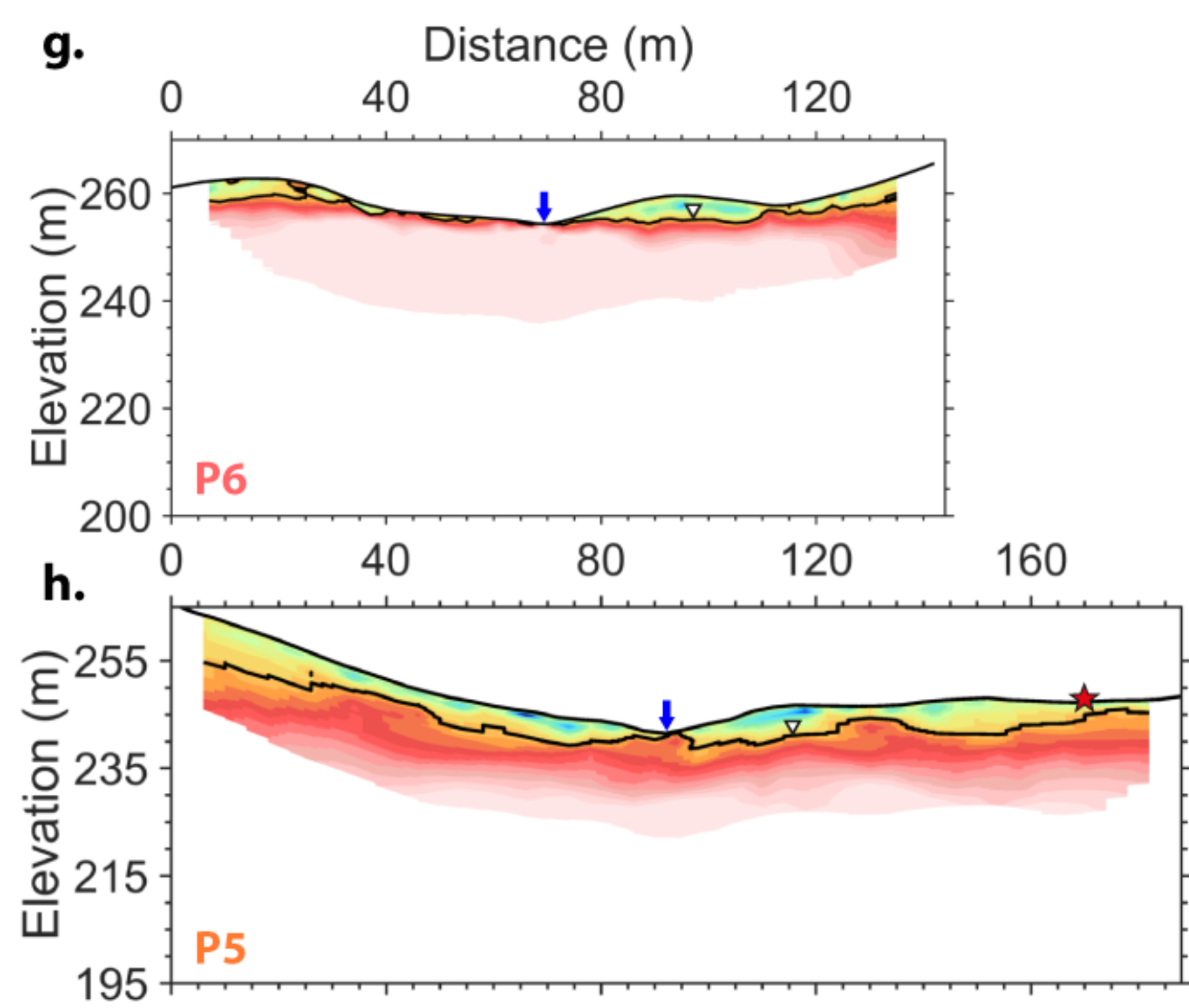
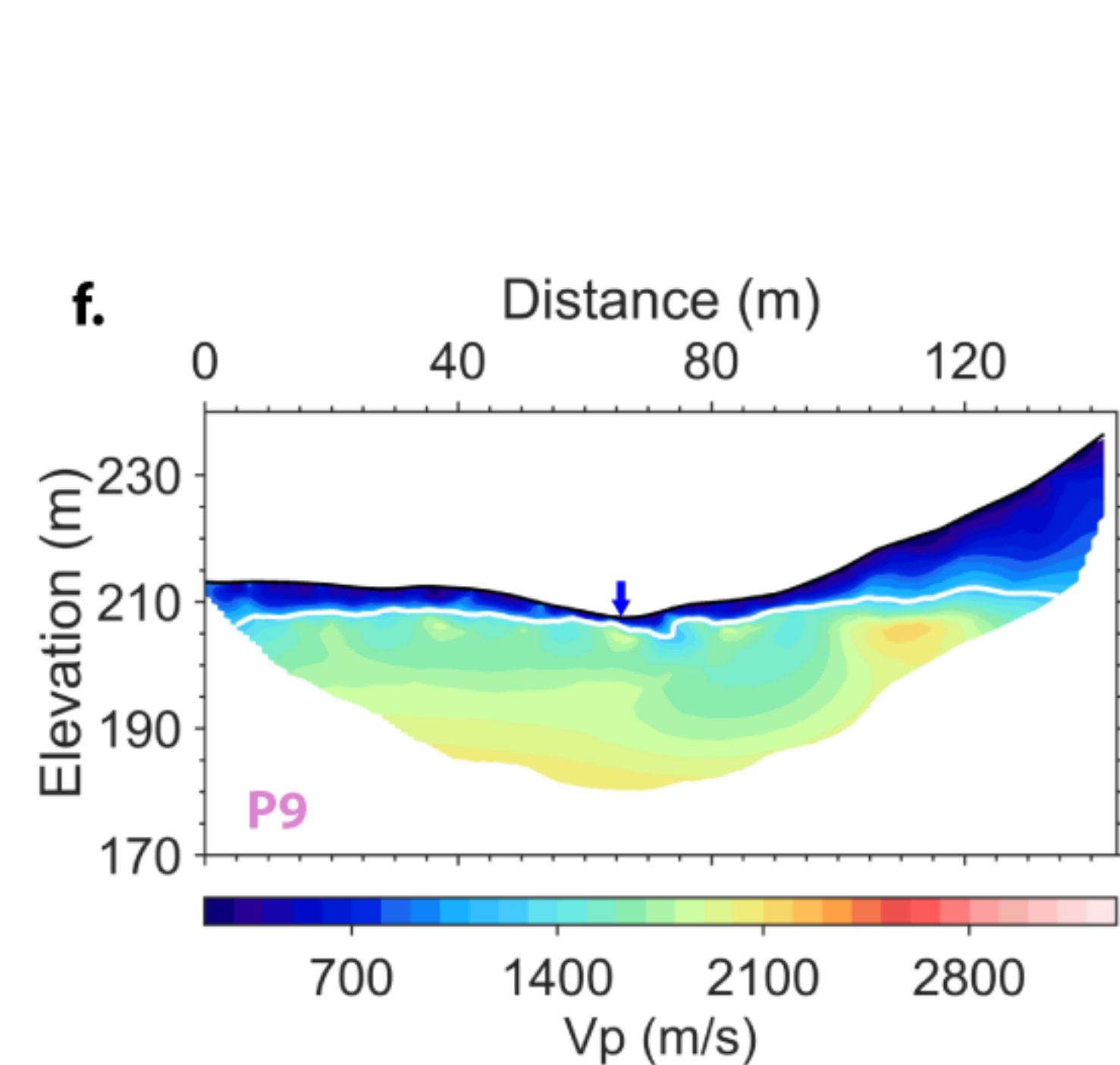
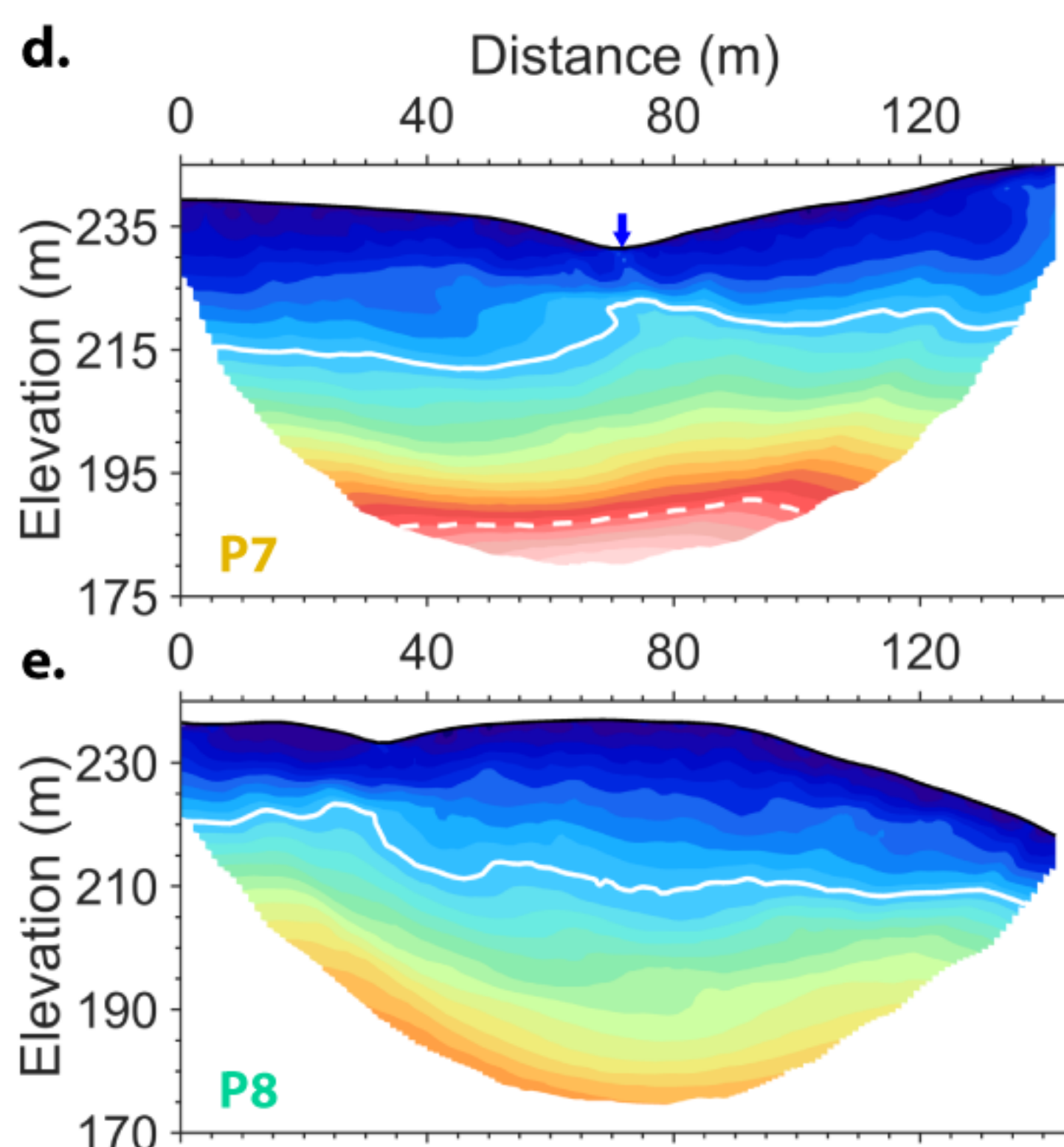
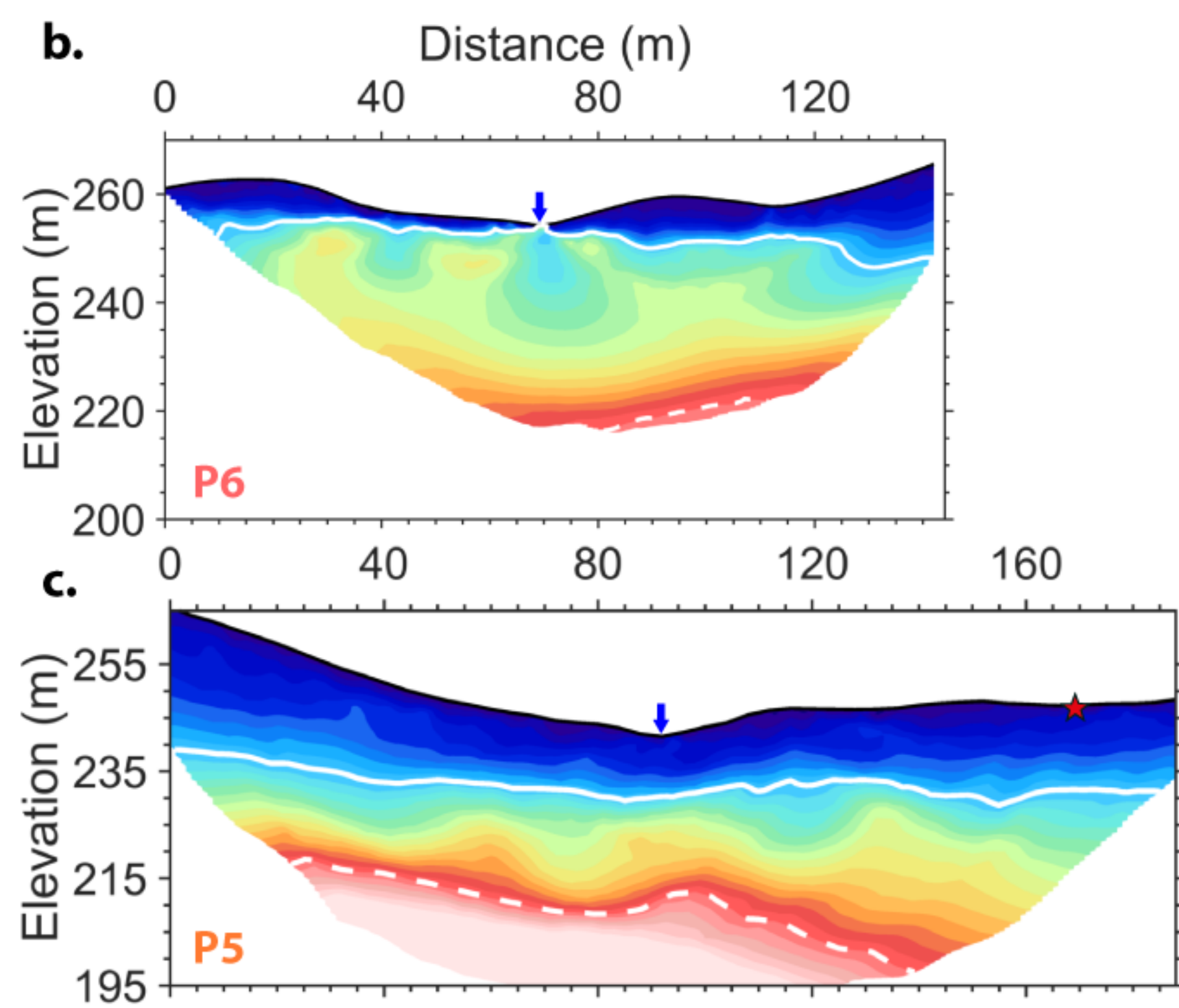


Figure 3.

